



# IGC Newsletter



## New Year Message

## Technical Articles

- Sensors for Comprehensive Monitoring of Hydrogen in Liquid Sodium and in Argon Cover Gas over Sodium
- Design and Development of Hydrostatic Pressure based Liquid Level Measurement System

## Young Officer's Forum

- Multiferroicity induced in  $GdMnO_3$  by 30% Y substitution

## Young Researcher's Forum

- Light-Matter Interaction of Sub-diffraction Limited Nanostructures

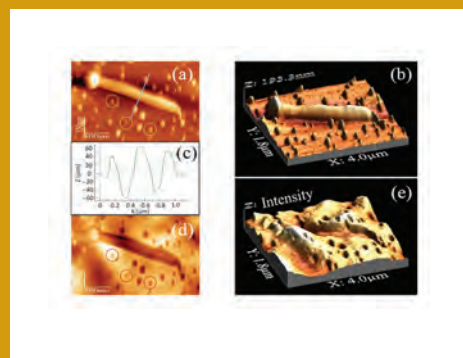
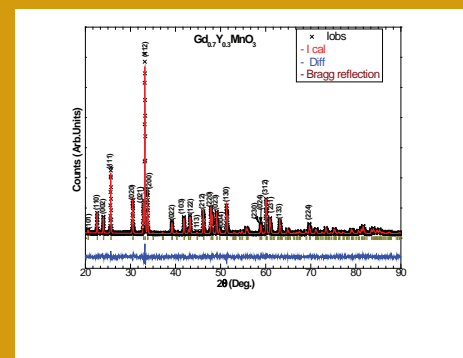
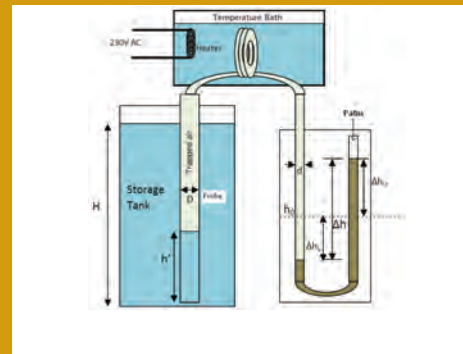
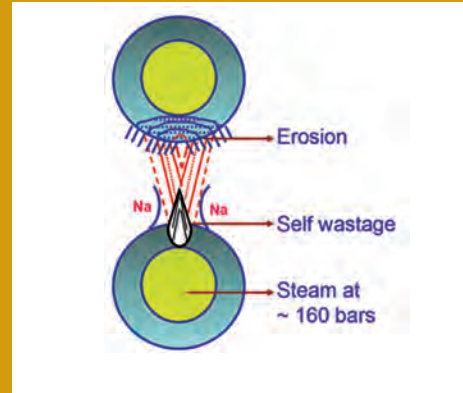
## Conference and Meeting Highlights

- 13<sup>th</sup> CEA-IGCAR Annual Meeting on LMFBR Safety
- National Conference on Condition Monitoring (NCCM-2017)
- 9<sup>th</sup> National Conference on Thermo Physical Properties
- The 2<sup>nd</sup> Research Coordination Meeting of the IAEA Coordinated Research Project (CRP)
- Theme Meeting on "Structural Integrity Assessment of Engineering Components"

## News and Events

## HBNI-IGCAR Corner

## Awards & Honours



## *From the Editorial Committee*

*Dear Reader*

We take this opportunity to wish you all a very Happy New Year, 2018.

It is our pleasant privilege to forward a copy of the latest issue of IGC Newsletter (Volume 115, January 2018 issue).

In this issue, we have introduced a new column HBNI-IGCAR Corner which will feature activities related to HBNI at IGCAR.

In the first technical article Dr. V. Jayaraman and colleagues from Materials Chemistry & Metal Fuel Cycle Group have shared their experience on Sensors for Comprehensive Monitoring of Hydrogen in Liquid Sodium and in Argon Cover Gas over Sodium.

In the second technical article Shri K. Praveen and colleagues from Electronics and Instrumentation Group have discussed about the Design and Development of Hydrostatic Pressure based Liquid Level Measurement System.

This issue's Young Officer's Forum features an article by Dr. R. M. Sarguna discussing about the Studies on Multiferroicity induced in  $\text{GdMnO}_3$  by 30% Y substitution.

Dr. A. K. Sivadasan has discussed on Light-Matter Interaction of Sub-diffraction Limited Nanostructures in Young Researcher's Forum.

We had distinguished visitors to our Centre in the last quarter, a delegation from CEA, France, and Dr. M. R. Srinivasan, Member, Atomic Energy Commission and former Chairman, Atomic Energy Commission.

We are happy to share with you the awards, honours and distinctions earned by our colleagues.

We look forward to your comments, continued guidance and support.

With best wishes and personal regards

Editorial Committee, IGC Newsletter

## New Year Message

### Dear Colleagues,

I wish all colleagues of Indira Gandhi Centre for Atomic Research (IGCAR) and General Services Organisation (GSO) and their families, a very happy, prosperous, fruitful and professionally enjoyable New Year 2018 and Season's Greetings for Pongal.

As we ushered in the New Year, we can look back the progress and accomplishments with respect to the various mission programs with a sense of satisfaction, identify the areas that need to be addressed, prioritise our works so that 2018 turns out to be far more satisfying experience.

In the year 2017, the flagship of our Centre - FBTR - reached its highest power level of 27.3 MWt during the 25<sup>th</sup> campaign generating an electrical power of - 6.0 MWe with the central experimental sub-assembly and one Mark-II fuel sub-assembly reaching its target burnup. FBTR continued to play an important role in testing of the fuels, structural materials and special neutron detectors for the FBR programme. KAMINI reactor was upgraded with a state-of-the-art single embedded system for reactor regulation purpose. It continues to provide excellent services for testing of pyro-devices for Indian space programs and also for activation analysis and irradiation of various samples.

IGCAR continued to provide the technical and manpower expertise in commissioning of PFBR. The synergism between IGCAR and BHAVINI has enabled commissioning of many support systems for PFBR. These include seismic qualification of important reactor systems, structural analysis, commissioning and performance checking of various component handling systems etc. For the future FBRs, detailed design studies, neutronics, structural, thermal hydraulics and safety analyses were taken up towards finalizing and firming up the design. This has contributed to significant progress in the design aspects. The work on FBTR-2, aimed towards having a 'fast spectrum test reactor facility' as a replacement for the present FBTR, with metal fuel as the driver fuel, has taken further steps. After detailed assessment of different options, functionally FBTR-2 is recommended for power generation.

It is satisfying to note that CORAL facility has completed the original mandate of reprocessing of 14 spent fuel sub-assemblies as licensed by the regulators, and has achieved its objectives of validation of the process and equipment developed for fast reactor fuel reprocessing.

Construction activities in FRFCF has progressed well with completion of cumulative concreting of -1.4 lakh cubic metres. The construction of infrastructure facilities and utility buildings were completed. On the housing front, GSO is playing a pivotal role in construction of 5 tower blocks consisting of 600 dwelling units.



Towards human resources development, BARC Training School at IGCAR successfully completed its 11<sup>th</sup> year and 33 young trained scientists and engineers were placed in various units of DAE. 32 JRFs of HBNI also attended their course work. It is indeed a matter of pride that about 450 students have graduated from BARC Training School at Kalpakkam. IGCAR continued to support the visits of engineering and post-graduate science students from various institutions across the country and also providing projects/internships for them. This in a great way helped the academic programs of universities and colleges which is one of the objectives of our Department.

Material procurement and purchase procedures have been further streamlined with the formation of Procurement Cell. The reconstituted Technology Transfer Cell has been given a mandate of transferring the potential technologies available at IGCAR to industries through a coordinated approach with DAE. The public awareness team of IGCAR made its impact in the 3<sup>rd</sup> India International Science festival.

The management functions in IGCAR & GSO has been rationalised and harmonized through a major restructuring for effective planning and execution under the various Vision Programs of the DAE. This would facilitate timely and expeditious processing of various administrative/executive proposals and would ensure proper and optimum utilisation of manpower, materials and facilities available in IGCAR & GSO as also provide opportunity for a constant and critical review of the scientific programs of IGCAR and projects & activities of GSO. This necessitated reconstitution of the IGCSC and formation of Group Boards across IGCAR & GSO as also formation of Group Program/activities committees as a mechanism for review and monitoring of the programs and activities of IGCAR & GSO. The formation of Group Boards was also essential for functionalising the new Peer Review Selection system for the Scientific/Technical Officers of Grades D and F.

The Administration and Accounts of both IGCAR & GSO did a commendable job in smooth execution of various projects and R&D programs and also in the timely rollout of pension arrears and implementation of seventh pay commission. Both these units were among the first within DAE to complete these mandates.

All the above would not have been possible without the dedicated efforts of our scientific, technical, administration, accounts and auxiliary cadres for which they well deserve all the appreciations.

The roadmap of 2018 is more challenging. We need to coherently synergise with BHAVINI to ensure completion of the commissioning of PFBR, which would be a landmark-event for the rollout of the second stage of DAE's nuclear power program. On the top of our priorities would also be the hot commissioning of DFRP and also finalising the preliminary design for FBR 1&2, the conceptual design of FBTR-2, including getting the necessary administrative and regulatory approvals. We also would have to finalise the completion of Sodium Technology Complex, Pyro Processing Engineering Facility and component testing plans for future FBRs. FBTR will go through its 26<sup>th</sup> campaign aiming a power generation of 32 MWt, irradiation of various combination of U-Pu-Zr pins and long term experiments of reactor structural materials. It is also our vision to transform the Central Workshop to a Centre for Advanced Manufacturing.

GSO has been taking great efforts for major upgradation of health care facilities. An outsourced pharmacy would be put in place and we would be operationalising the CHSS facility at IMSc Chennai complex.

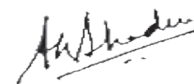
All efforts, with full support at all levels in DAE and State Administration, are being undertaken for markedly improving the

security of the residential colonies at Kalpakkam and Anupuram in full harmony with the neighbourhood and with the full support of CISF through enhanced deployment of security personnel.

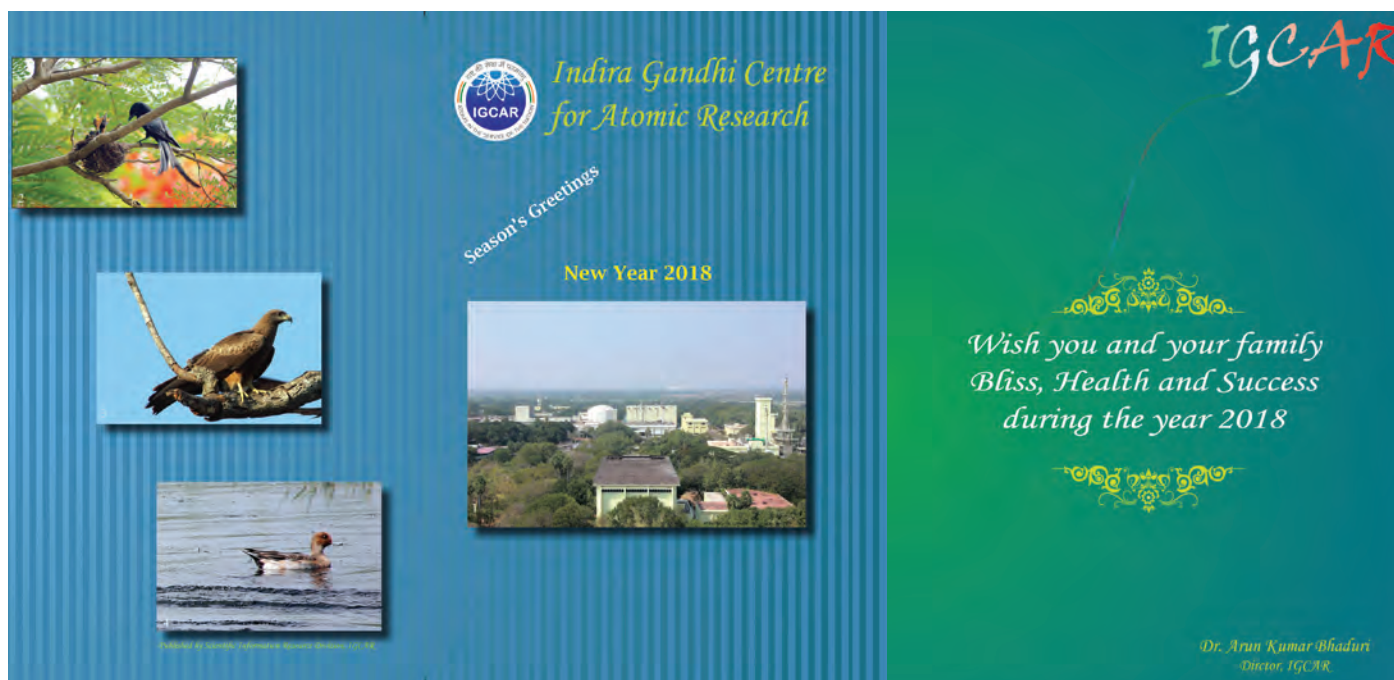
The principals, teachers and staff as also students and their parents of the 2 Kendriya Vidyalayas and 3 Atomic Energy Central Schools deserve our compliments for continuing improved performance in the X & XII Board Examinations. GSO continued to provide excellent support at improving the amenities at all the 5 schools. It has been possible to provide the wards of our colleagues, admission to the CBSE syllabus based education for the + 1 students. It has been our endeavour to provide transparent, discretion-free admissions at all levels in the schools including admissions to the neighbourhood children as a part of our Corporate Social Responsibility, a practice which we would continue to do in the forthcoming academic year as well.

It will continue to be our endeavour to enable younger colleagues across all cadres of IGCAR & GSO to enable them to take higher responsibilities in the mission based programs and activities of both the units. All this would enable us to sustain the excellence in the domain of fast reactor and associated fuel cycle technologies.

I look forward to work very closely, through an interactive and transparent mechanism, with all our scientific, technical, administrative, accounting, auxiliary and security colleagues.



(Arun Kumar Bhaduri)  
Director, IGCAR



## Sensors for Comprehensive Monitoring of Hydrogen in Liquid Sodium and in Argon Cover Gas over Sodium

Sodium in large volumes is being used as the heat transfer medium in fast breeder reactors. Heat energy from the nuclear reaction is carried by sodium and transferred to steam, in the steam generator, across 3-4 mm wall thickness of ferritic steel tubes. Figure 1 shows the schematics of a typical steam generator of sodium cooled fast reactor. Liquid sodium circulates in shell side and water circulates in counter direction in a tube configuration.

Any defect in these tubes, will lead to the leak of high pressure steam into sodium at high temperatures, resulting in sodium – water reaction (Figure 2). This interaction leads to the instantaneous evolution of hydrogen and sodium hydroxide. As seen from the figure, high pressure steam present in the tube would leak into sodium like a jet of stream. There could be self-wastage due to corrosive nature of NaOH, which widens the leaking area and further erode the neighbouring tubes as a result of large pressure gradient as well as the caustic nature of the product formed. This eventuality of steam leak into sodium is to be detected at its incipient stage itself, in order to avoid prolonged and cost intensive shutdown of the reactor. Monitoring of hydrogen and oxygen levels in sodium and/or argon cover gas depending on the operating conditions of the reactor, will help early stage identification of steam leak in sodium. Sensors that have been developed for detecting hydrogen towards this goal are:

1) During normal operating conditions of the reactor, the sodium temperature is above 450°C and the hydrogen formed as a result of the sodium-steam reaction will dissolve in sodium. Monitoring hydrogen level in sodium will provide information of such a leak.

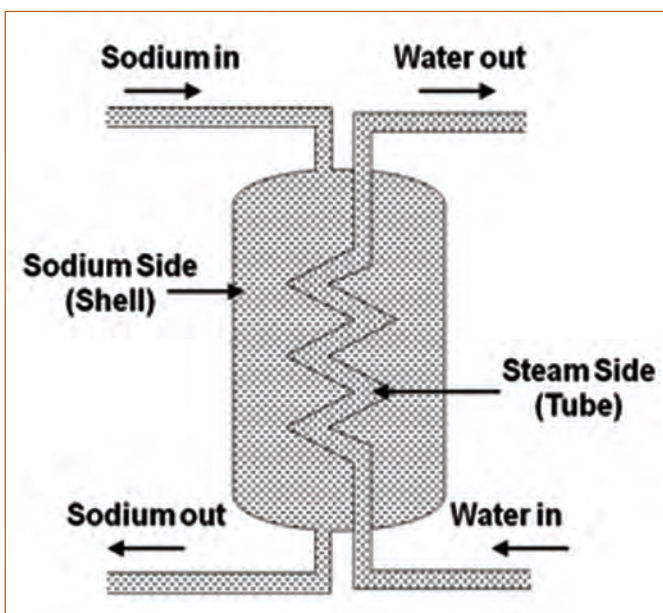


Figure 1: Typical schematic diagram of the steam generator

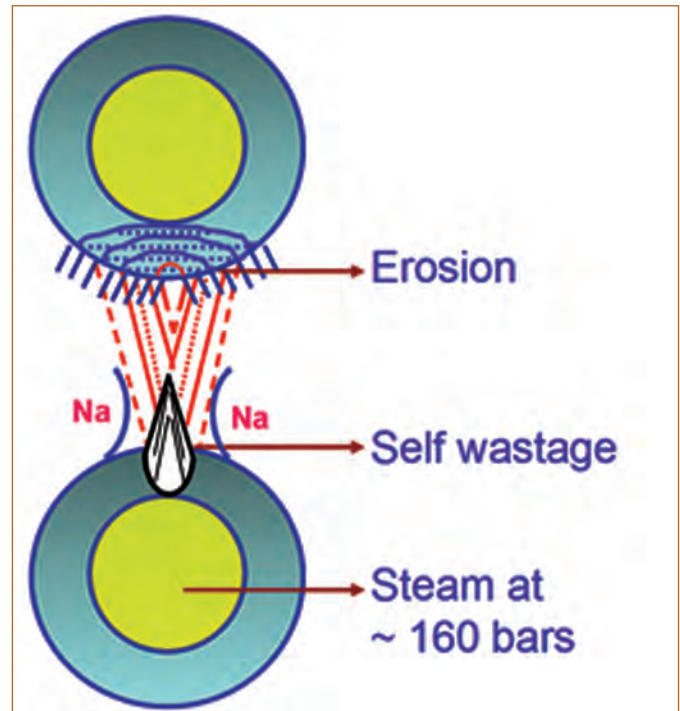


Figure 2: Typical scenario of steam leak in the steam generator module

Towards this purpose an electrochemical hydrogen meter (ECHM) to monitor the sodium circuit for hydrogen is developed.

2) During start-up and low power operation of the reactor, the sodium temperature is maintained below 250°C normally, and the hydrogen formed in the above reaction escapes to the argon cover gas plenum present over sodium. Diffusion based hydrogen monitoring system comprising thermal conductivity detector (TCD) coupled with surface conductivity sensor (tin oxide sensor) is developed for using them as cover gas monitoring system.

### Scheme of the hydrogen detection system

All hydrogen detecting systems such as ECHM, TCD based hydrogen detection system and tin oxide sensor, consist of three main parts as shown in Figure 3. The hydrogen detecting system produces an output in volts, which is related to the hydrogen concentration. The signal is amplified in the preamplifier assembly and transmitted as frequency signal. Microprocessor provided in the display unit processes the sensor signal suitably, correlate to the hydrogen concentration and makes it available for recording. All the mechanical, electrical, electronics and instrumentation

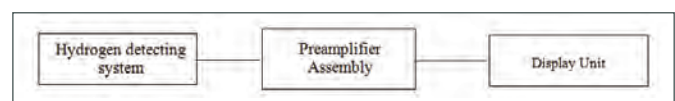


Figure 3: Block diagram of the hydrogen detection system

needed have been designed in-house, developed and field tested. They have undergone seismic qualification test as stipulated by AERB.

**Electrochemical hydrogen meter (ECHM)**

Electrochemical hydrogen meter offers an attractive alternate technology to the conventional diffusion based hydrogen meter (CDHM) employed in fast reactors, due to its simplicity, compactness and requirement of minimum maintenance work. CDHM works on dynamic mode whereas ECHM works on equilibrium mode. ECHM is an electrochemical concentration cell and can be used to measure the hydrogen present in sodium against a reference hydrogen partial pressure under equilibrium mode.

ECHM uses  $\text{CaBr}_2\text{-CaHBr}$  biphasic mixture as the electrolyte which conducts only  $\text{H}^-$  ions. This electrolyte has been chosen based on investigations of several alkali and alkaline earth metal halide and hydride systems, carried out over three decades in our Centre. A mixture consisting of calcium and magnesium along with calcium hydride is used as the reference electrode that fixes the hydrogen partial pressure of reference side at the meter operating

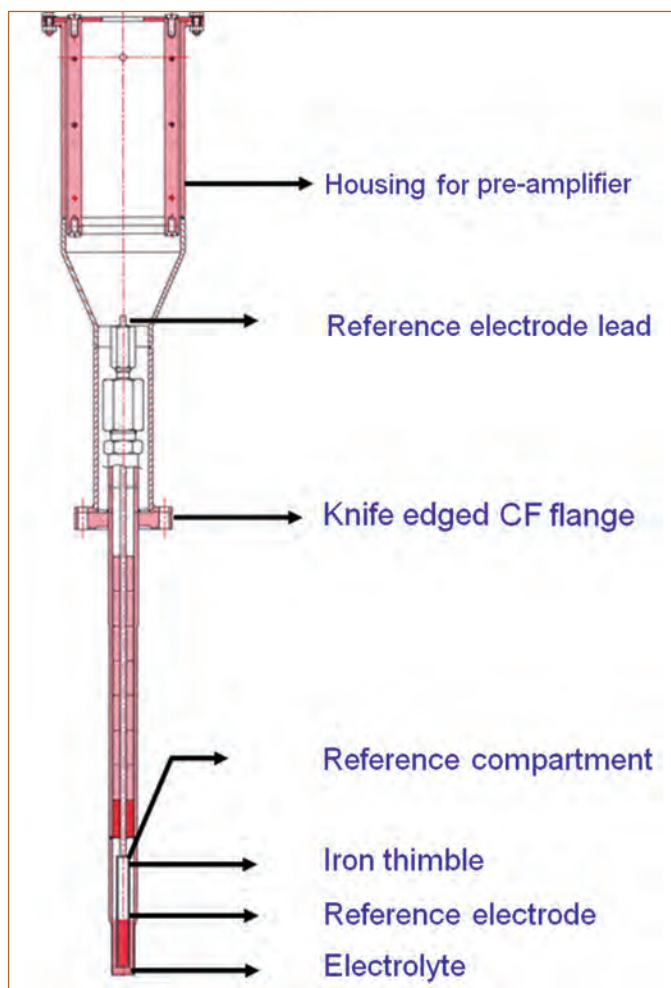


Figure 4: Schematics of electrochemical hydrogen meter

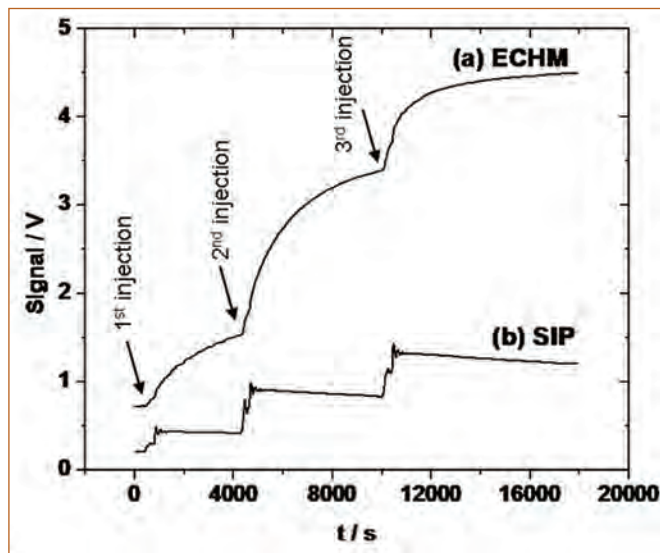


Figure 5: Typical response of ECHM along with SIP for three times of 40 ppb hydrogen injection into sodium at 450°C in FBTR

temperature. Hydrogen concentration in sodium fixes the hydrogen partial pressure of sample side. The meter operating temperature has been chosen as 450°C.

**Configuration of the ECHM system**

A schematic diagram of the ECHM is shown in Figure 4. The meter consists of a pure iron thimble for housing the electrolyte and another pure iron thimble for holding the reference electrode materials. The electrolyte thimble is then welded to a stainless steel pipe, which in turn is welded to a knife-edged flange. The electrolyte cast from its molten state fills up the annular gap between the two iron thimbles. The space between electrolyte compartment and the electrode compartment is filled with alumina spacers for aligning the reference electrode at the center of the electrolyte compartment.

Assembling of ECHM (Figure 4) involves several steps, namely: (i) fabrication of components, (ii) orbital welding of SS pipe with pure iron thimble, (iii) quality check of the assembled components, such as radiography and helium leak testing, (iv) preparation and purification of air/moisture sensitive electrolyte and electrode materials, (v) welding of reference electrode assembly inside argon atmosphere glove box, (vi) assembly of electrochemical cell and pore-free casting of electrolyte, (vii) quality check of the ECHM using radiography.

The meter has been calibrated as a function of hydrogen concentration in sodium in a bench top sodium loop. The calibration constants are entered into the display unit and the output is displayed by a digital potentiometer in concentration units of parts per billion (ppb) of hydrogen in sodium. The same output is available for recording from the rear panel of the display unit.

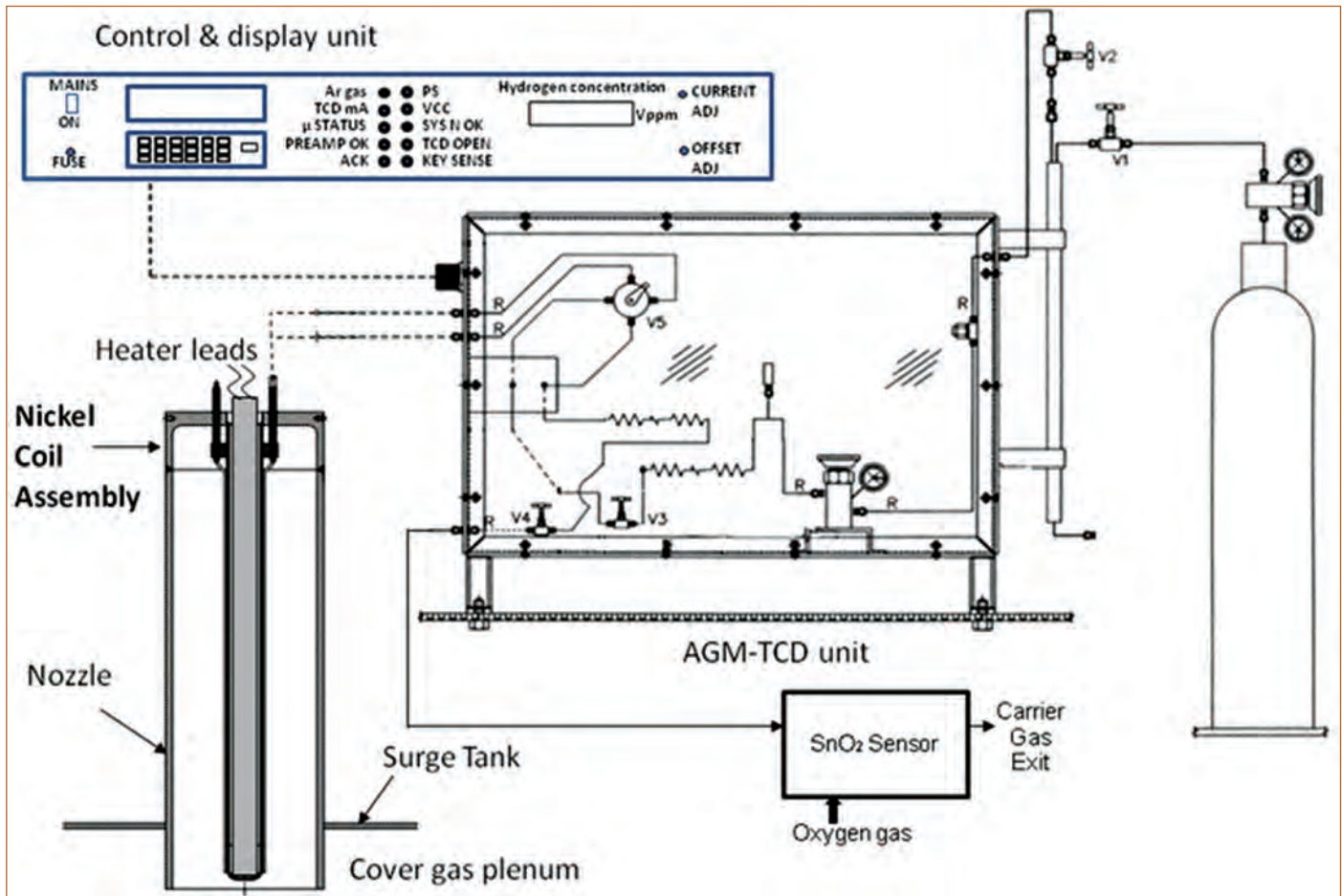


Figure 6: Schematics of diffusion based hydrogen detector and Sn<sub>2</sub> sensor

ECHMs are installed in FBTR and various sodium facilities of IGCAR such as SGTF, SOWART. ECHMs were also installed in Phenix reactor and Cadarache sodium loop in France, as part of IGCAR-CEA collaboration on fast reactor safety. A typical response of ECHMs for hydrogen injection of 40 ppb along with conventional nickel membrane based sensor sputter ion pump (SIP) detector is shown in Figure 5, during one of the hydrogen injection tests in FBTR. It can be seen from the figure that the response behavior of ECHM is in tandem with that of the SIPs.

**Diffusion based hydrogen monitoring system using TCD**

Hydrogen possesses low mass and size and can diffuse through metal and also has higher thermal conductivity, nearly 10 times higher than argon. Hence TCD based hydrogen sensor system is designed to monitor the hydrogen level in cover gas plenum in expansion tank of secondary sodium loop. It consists of a nickel diffuser / nickel coil assembly (NCA), argon gas manifold (AGM)-cum-TCD unit and control & display unit. Figure 6 shows the schematic of hydrogen in argon detector (HAD) system. Fabrication of the nickel coil assembly, involves the bending of 0.25 mm wall thickness and 1 m length nickel tubes, in U shape and fastening them over one end closed SS central pipe. The ends

of the nickel tubes are welded to the grooved flange through a SS sleeve. The inlet and outlet tubes from the grooved-flange are then welded to the top flange. Quality checks, such as radiography and helium leak testing are required to be undertaken during every step of fabrication process. The qualified nickel diffuser is integrated with the expansion tank of secondary sodium loop and maintained at 500°C. It is used to separate the hydrogen, which is released during sodium – water reaction, from the argon cover gas present over sodium in expansion tank. Argon carrier gas is used to sweep away diffused hydrogen from the diffuser membrane. The flow rate of argon carrier gas is regulated at 30 ml/min in AGM-cum-TCD unit and passed through reference compartment and then to the nickel coil assembly in order to sweep away any hydrogen present in the nickel tube to the sample compartment of TCD. A constant current is supplied to TCD by means of micro controller based control & display unit. The signal from TCD is amplified and processed in control & display unit as shown in Figure 3.

**Characteristics of TCD based hydrogen detection system**

Thermal conductivity detector based hydrogen sensor system is calibrated between 50 and 1000 vppm using calibrated gas mixtures streaming over the nickel diffuser which is maintained

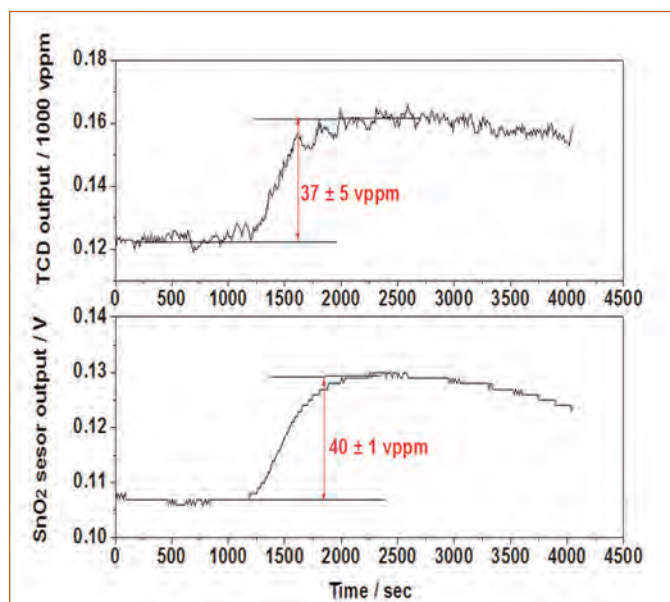


Figure 7: Typical response characteristics of TCD and SnO<sub>2</sub> sensors towards steam injection experiment in SOWART at sodium temperature of 250°C

at 500°C and the response of the TCD based hydrogen sensor system is recorded. As the mass flow rate of the argon carrier gas varies with change in ambient temperature, the response of TCD based hydrogen sensor system is observed with large oscillation over a day. Hence the temperature coefficient of the TCD signal is obtained from the data of the signal with respect to ambient is incorporated in the software of microcontroller based control & display unit to correct the signal. After implementation of correction factor, the oscillation of the signal is observed within 30 vppm of hydrogen in argon. The instantaneous noise is found to be  $\pm 10$  vppm of hydrogen in argon. Taking the signal to noise ratio as 3, the minimum detection limit of TCD based hydrogen sensor system is found to be 30 vppm. Calibration of the TCD based hydrogen detection system shows linear response with injected hydrogen concentration.

In order to bring down the minimum detection limit of diffusion based hydrogen monitoring system to 1 vppm, surface conductivity based hydrogen sensor system is developed to couple with this system.

#### Surface conductivity based hydrogen sensor system

It is well known that the surface electrical conductivity of some semiconducting oxides viz. SnO<sub>2</sub>, ZnO, etc. gets significantly altered in presence of trace levels of reducing/oxidizing analyte gas in ambient air, but gets restored to the original value when the trace analyte gas is removed from the ambient. This property can be exploited for monitoring trace levels of hydrogen in argon cover gas. Towards this application, a thin film of tin oxide is deposited

on one side of an alumina substrate with printed platinum heater on the other side. Using the platinum heater provided on the rear side of the substrate, sensor is maintained at 350°C. The sensor housing is  $\sim 10$  ml with provisions for gas inlet and outlet.

#### Integration of TCD based hydrogen detection system with tin oxide sensor

Tin oxide sensor is positioned in the sample side argon vent of TCD based system, which is mixed with oxygen such that the overall oxygen concentration in the stream is 21% O<sub>2</sub>. The synthetic air composition (Ar + O<sub>2</sub>) is allowed to enter into the SnO<sub>2</sub> sensor as shown in the schematic in Figure 6.

#### Characteristics of tin oxide based sensors

Tin oxide sensor is calibrated towards H<sub>2</sub> between 5 and 100 vppm. The calibration plot is fitted to a first order polynomial. The baseline stability of the sensor is measured for about 100 h and the mean background voltage shown by the sensor is deduced, which corresponded to less than 1 vppm of hydrogen in argon. The minimum detection ( $3\sigma$ ) and quantification ( $10\sigma$ ) limit shown by SnO<sub>2</sub> sensor towards H<sub>2</sub> are 1 vppm and 9 vppm, respectively.

#### Performance of TCD and tin oxide sensors based hydrogen detection system towards hydrogen and steam injections in SOWART

Performance of the TCD and tin oxide sensor based hydrogen detection system is evaluated by injecting hydrogen or steam in sodium water reaction test rig (SOWART). These injections were carried out in sodium. Hydrogen injection experiments were carried out by maintaining sodium at different temperatures ranging from 180 to 250°C, in order to simulate low power operating conditions of the reactor. Hydrogen injection experiments proved that this sensor responded down to 5 vppm level of hydrogen in argon and is possible to detect up to 100 vppm reliably, which correspond to steam / water leak of a few tens of milligrams ( $10^{-2}$  g) in the facility ( $10^6$  g of sodium). Steam injection experiments were carried out by maintaining sodium temperature at 250°C. Figure 7 shows the typical simultaneous response characteristics of TCD and SnO<sub>2</sub> sensor, during one of the steam injection experiments in sodium. It can be seen that both sensors showed the value of about 40 vppm of hydrogen in argon indicating good correlation of the values obtained.

#### Simultaneous response of sensors

The presence of in-sodium hydrogen sensor, namely ECHM as well as cover gas hydrogen sensors, namely both TCD and SnO<sub>2</sub> sensors, covering a wider hydrogen concentration range, in a sodium facility helps in understanding the nature of steam leaks. Depending on the temperature of sodium and extent of steam leak, the response behaviour of these sensors differs.



Table : Summary of various scenarios of steam leaks and the expected response behaviour of hydrogen sensors

Sodium temperature /°C	Hydrogen concentration during steam leak	Expected response behaviour		
		ECHM	TCD	SnO <sub>2</sub>
250	10-100 vppm in cover gas	*	Low	Good
	100-1000 vppm in cover gas	*	Good	Good
450	10-200 ppb	Good	Low	Low
	>200 ppb	Good	Good	Good

\* Hydrogen evolved escapes to cover gas at sodium temperature < 250°C as the dissolution of it in sodium is kinetically hindered

Figure 8 shows the simultaneous response of all the sensors during a simulation experiment in SOWART for a steam leak (approximately, > 1000 ppb of hydrogen) into sodium circuit with sodium maintained at 450°C. As seen from the figure, a large fraction of hydrogen evolved as a result of sodium – water reaction dissolved into liquid sodium and ECHM responded instantly and reaches saturation limit corresponding to 1400 ppb of hydrogen in sodium. A small fraction of un-dissolved hydrogen escapes into the cover gas plenum. Considering the length of the sodium circuit and the flow rate of liquid sodium, a travel time of approximately 500 seconds is worked out for the undissolved hydrogen to reach the cover gas plenum, from the actual site of steam leak. Gradual build up of hydrogen level in cover gas plenum takes place and the diffusion of hydrogen across the nickel membrane starts

which in turn is swept away by a stream of argon. This hydrogen in argon is detected both by TCD and SnO<sub>2</sub> sensors. Taking into account, the transportation of hydrogen by the sodium and argon streams successively in addition to its diffusivity across the nickel membrane, the TCD and SnO<sub>2</sub> sensors respond after a delay time of 800 seconds. Moreover, unlike the abrupt change in signal from ECHM which measures the changes in partial pressure of hydrogen in equilibrium with the liquid sodium, a gradual increase in signal strength is observed from both TCD and SnO<sub>2</sub> sensors although the response is simultaneous. From the calibration graphs of TCD and tin oxide sensors, the concentration of hydrogen reached in cover gas plenum is deduced to be ~ 40 vppm.

The results obtained from these R&D activities demonstrate the usefulness of hydrogen detection system for monitoring low levels of hydrogen both in sodium or argon cover gas over sodium system during steam leak in the steam generator of FBRs. Calibration plot of ECHM shows its worthiness in determining the hydrogen concentration in the range of 50 to 500 ppb with a resolution of 5% of the display value. TCD based hydrogen detection system is useful to detect the hydrogen concentration in argon cover gas in the range of 30 to 3000 vppm. The tin oxide sensor responded for hydrogen injection down to 5 vppm of hydrogen in argon and is possible to detect up to 100 ppm reliably. Required numbers of ECHMs and CGHMs are ready for deployment in PFBR, presently.

Authors thank the colleagues of FBTR, SOWART and SGTF of IGCAR and Phenix reactor and SPERFENENEC sodium loop in France for their support during the installation and monitoring the performances of sensors. Authors are also thankful to the colleagues of CWD, QAD, REG for their support in fabrication, quality control and seismic testing, respectively.

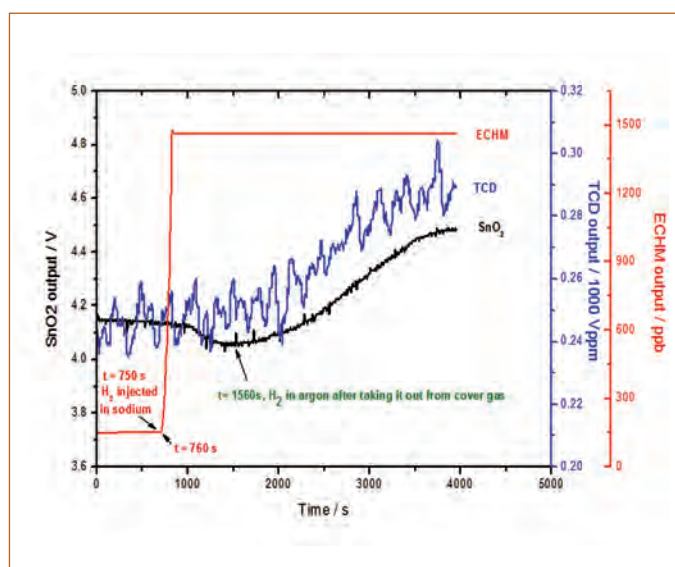


Figure 8: Simultaneous response of (a) ECHM, (b) TCD and (c) SnO<sub>2</sub> hydrogen sensors for a steam leak of higher concentration at high temperature in SOWART

V. Jayaraman and colleagues  
Materials Chemistry & Metal Fuel Cycle Group

## Design and Development of Hydrostatic Pressure based Liquid Level Measurement System

Liquid level measurement (LLM) in storage tanks is one of the important process parameter that needs to be measured and controlled, in nuclear reactor and associated facilities. A novel approach towards deployment of a hydrostatic pressure based level measurement system is presented, for continuous monitoring of liquid level in a reservoir. This system is similar to conventional bubbler/purge method, but overcomes many of its drawbacks such as requirement of pressure sensor depending on range of measurement, bubbling effect by passing air or any gaseous fluid into the liquid, spurious information of measured level due to change in ambient temperature etc. In the present work, a capacitance based pulsating sensor is used to precisely measure hydrostatic pressure exerted by the process liquid and it is correlated to liquid level. In order to avoid strong influence of temperature on level measurement, a temperature compensation methodology is derived and used in the system. This technique is simple and reliable as it does not involve any moving parts. This can be used as an intrusive type level measurement with good accuracy for a wide range of ambient temperatures.

### Sensing Methodology

The principle of proposed technique involves sensing of liquid level by measuring hydrostatic pressure head exerted by process liquid. It is demonstrated using a storage tank with water as the process liquid and a simple oil manometer made of Perspex as the sensor, as shown in Figure 1. The hydrostatic pressure exerted by liquid is measured by dipping a hollow pipe from the top, referred to as probe, which runs till the bottom of tank. The top end of the probe is connected to a manometer using a flexible tube and the manometer is partially filled with a sealing liquid (low volatile mineral oil). A constant temperature bath is provided to vary the temperature for the trapped air inside the probe during experiment. Hydrostatic pressure exerted by water is expressed as

$$\text{Hydrostatic Pressure} = H * \rho * g \quad (1)$$

H: Water level in tank     $\rho$ : Density of water

g: Acceleration due to gravity

As the level in the tank increases, there will be a liquid ingress inside the hollow probe due to the compression of trapped air. So the actual pressure measured by the manometer is not exactly as per the relation given in Equation 1. When the tank is empty, oil level in both arms of manometer is same ( $\Delta h$  is zero) and denoted as  $h_0$ . The volume of air column from the bottom end of probe to oil surface of manometer at atmospheric pressure is denoted as  $V_{atm}$ . As the water level inside the tank becomes H, the manometer shows a deflection of  $\Delta h_1$  and there is a rise in the level inside the hollow probe denoted as  $h'$ . The hydrostatic

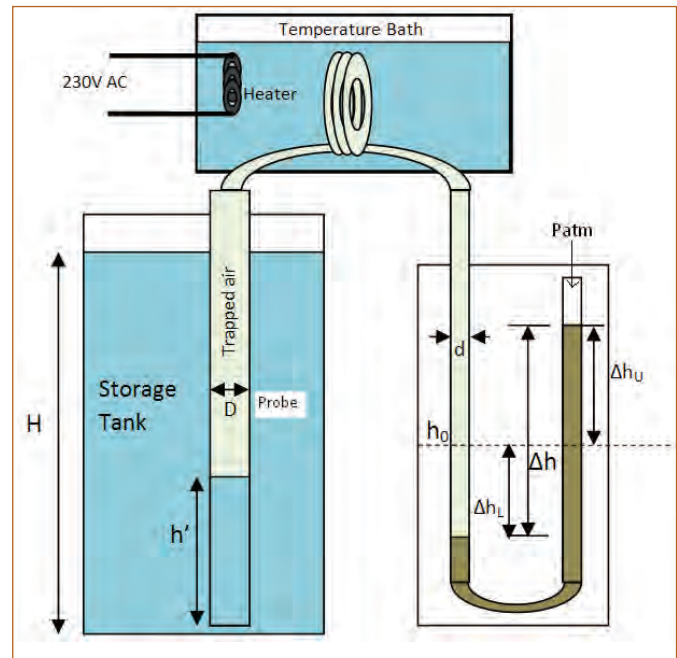


Figure 1: Setup for demonstration

pressure measured by the manometer is equal to the pressure exerted by the differential water level ( $H-h'$ ). This implies that, pressure exerted by total liquid level in the tank is not considered for level measurement. Rather the pressure developed due to difference in liquid level between the tank and the hollow dip probe is correlated to the actual liquid level in the tank. Hence, by selecting appropriate diameter of probe, the entire liquid level in tank can be scaled down to range of sensor. Considering constant ambient temperature and using Boyle's Law, relation between level H and manometer reading  $\Delta h$  is re-written as Equation 2. This equation is used to optimize the diameter of probe (D) for measurement level H using a sensor of  $\Delta h$  range.

$$H = \Delta h_1 [(\rho_o/\rho_w) + (d^2/D^2)] + [V_{atm} \cdot (P_{atm} \cdot V_{atm}) / P_1] \quad (2)$$

$\rho_w$  and  $\rho_o$  are density of water and oil respectively

$V_{atm}$ : Vol. of air column at atmospheric pressure

$P_{atm}$ : Atmospheric pressure

$P_1$ : Hydrostatic pressure at level H which is the sum of atmospheric pressure and  $\Delta h_1 * \rho_o * g$

### Temperature Compensation

In reality, change in ambient temperature leads to change in density of trapped air inside hollow probe. This air density variation is also reflected in  $\Delta h$  reading of manometer, which needs to be compensated. A methodology is formulated to relate level to  $\Delta h$  and temperature and verified experimentally using the setup shown in Figure 1.

Ideal gas law states that

$$PV = nRT \quad (3)$$

n: number of moles for trapped air R: Specific gas constant of dry air at STP, 287.05 J/Kg.K

When the tank is empty  $\Delta h = 0$

$$P_{atm}V_{atm} = nRT_0 \quad (4)$$

$P_{atm}$  : Atmospheric pressure

$V_{atm}$ : Volume of air column at atmospheric pressure

$T_0$ : Initial ambient temperature when  $\Delta h = 0$

Let us consider the condition when water is filled to a level of H keeping the temperature constant and the deflection in manometer reading becomes  $\Delta h_1$  and water ingress inside probe is  $h_1'$ . The trapped air pressure and density is given by

$$P_1 = P_{atm} + (\Delta h_1 * \rho_o * g) \quad (5)$$

$$\rho_{air1} = P_1/[R * (T_0 + 273.15)] \quad (6)$$

Now consider that ambient temperature is increased from  $T_0$  to  $T_2$  keeping water level same. The increase in temperature causes a change in trapped air density which in turn changes the volume of trapped air and finally  $\Delta h$  reading in manometer. Let the manometer reading be  $\Delta h_2$  and water ingress inside probe is  $h_2'$ . Neglecting the oil expansion, new trapped air pressure, volume and density given by

$$P_2 = P_{atm} + (\Delta h_2 * \rho_o * g) \quad (7)$$

$$V_2 = (P_{atm} * V_{atm} * T_2)/(T_0 * P_2) \quad (8)$$

$$\rho_{air2} = P_2/[R * (T_2 + 273.15)] \quad (9)$$

The change of manometer reading ( $\Delta h_2 - \Delta h_1$ ) is only due to the variation in ambient temperature and not due to change in level of water. Hence this change must be compensated to get an accurate measurement of level from manometer readings. In the actual scenario  $P_1$ ,  $V_1$  and  $\rho_{air1}$  are unknown values while  $P_2$ ,  $V_2$ ,  $\rho_{air2}$ ,  $T_2$ ,  $T_0$  and  $\Delta h_2$  are known values. It is assumed that the difference in air density at pressure  $P_1$  and  $P_2$  is negligible. This assumption is followed to determine the approximate air density at  $T_0$ .

$$\rho_{air1(appx)} = P_2/[R * (T_0 + 273.15)] \quad (10)$$

The approximate volume of trapped air at  $T_0$  at level H is given by

$$V_{1(appx)} = (\rho_{air2}/\rho_{air1(appx)}) * V_2 \quad (11)$$

Hence the change in volume of trapped air due to change in ambient temperature is

$$\Delta V_{(appx)} = V_2 - V_{1(appx)} \quad (12)$$

This change in volume of trapped air will change  $h_2'$  as well as  $\Delta h_2$  in such a way that it satisfies the new equilibrium condition

$$(H - h_2') * \rho_w * g = \Delta h_2 * \rho_o * g \quad (13)$$

where  $h_2'$  and  $\Delta h_2$  are the new values at  $T_2$ . From Equation 13,

the net change in  $h'$  ( $\partial h'$ ) and net change in  $\Delta h$  ( $\partial \Delta h$ ) due to change in temperature is related as

$$\partial h' = (\rho_o/\rho_w) * \partial \Delta h \quad (14)$$

Change in volume  $\Delta V_{(appx)}$  is distributed towards  $h'$  and  $\Delta h$  and it can be equated to

$$\Delta V_{(appx)} = [(\pi/4) * D^2 * \partial h'] + [(\pi/4) * d^2 * \partial \Delta h_L] \quad (15)$$

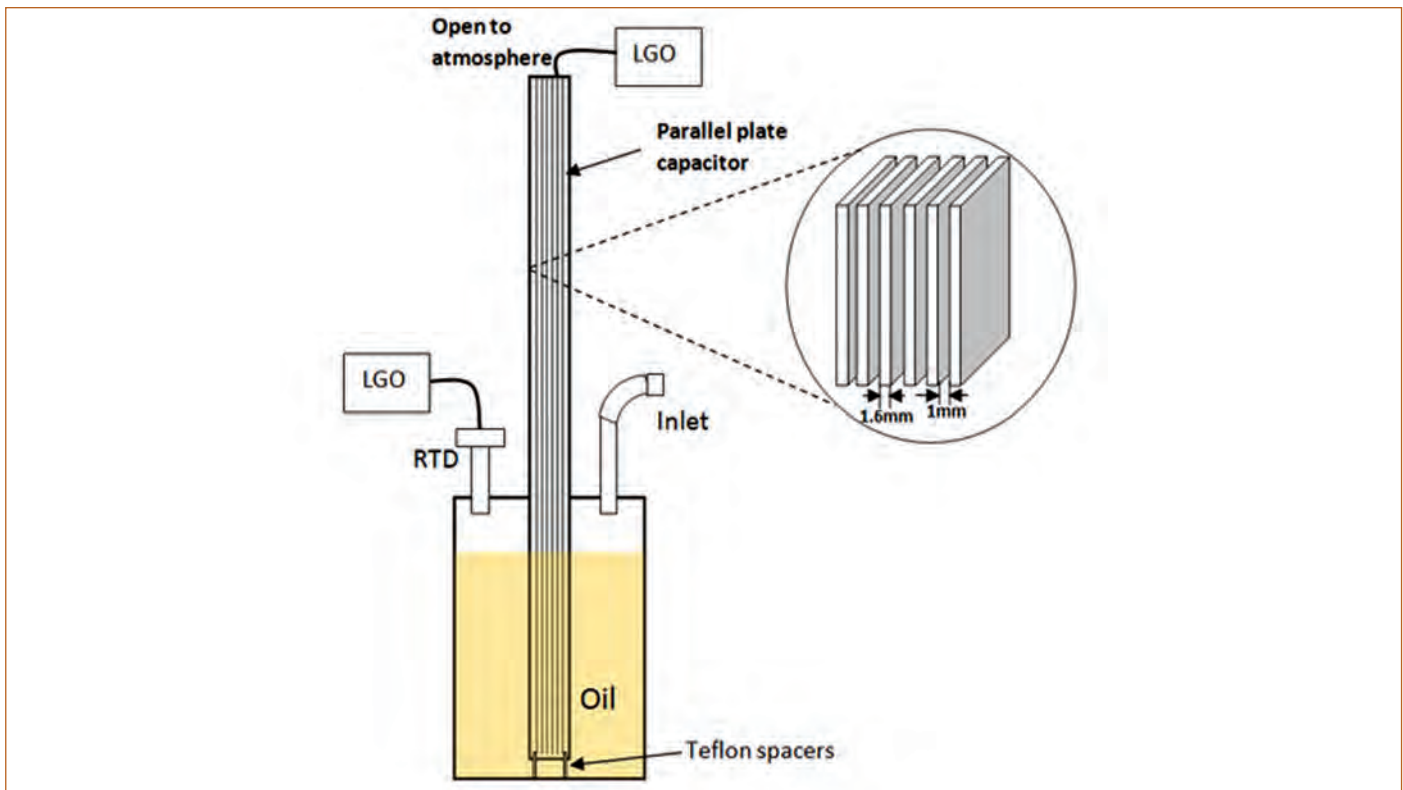


Figure 2: Topology of differential pressure pulsating sensor

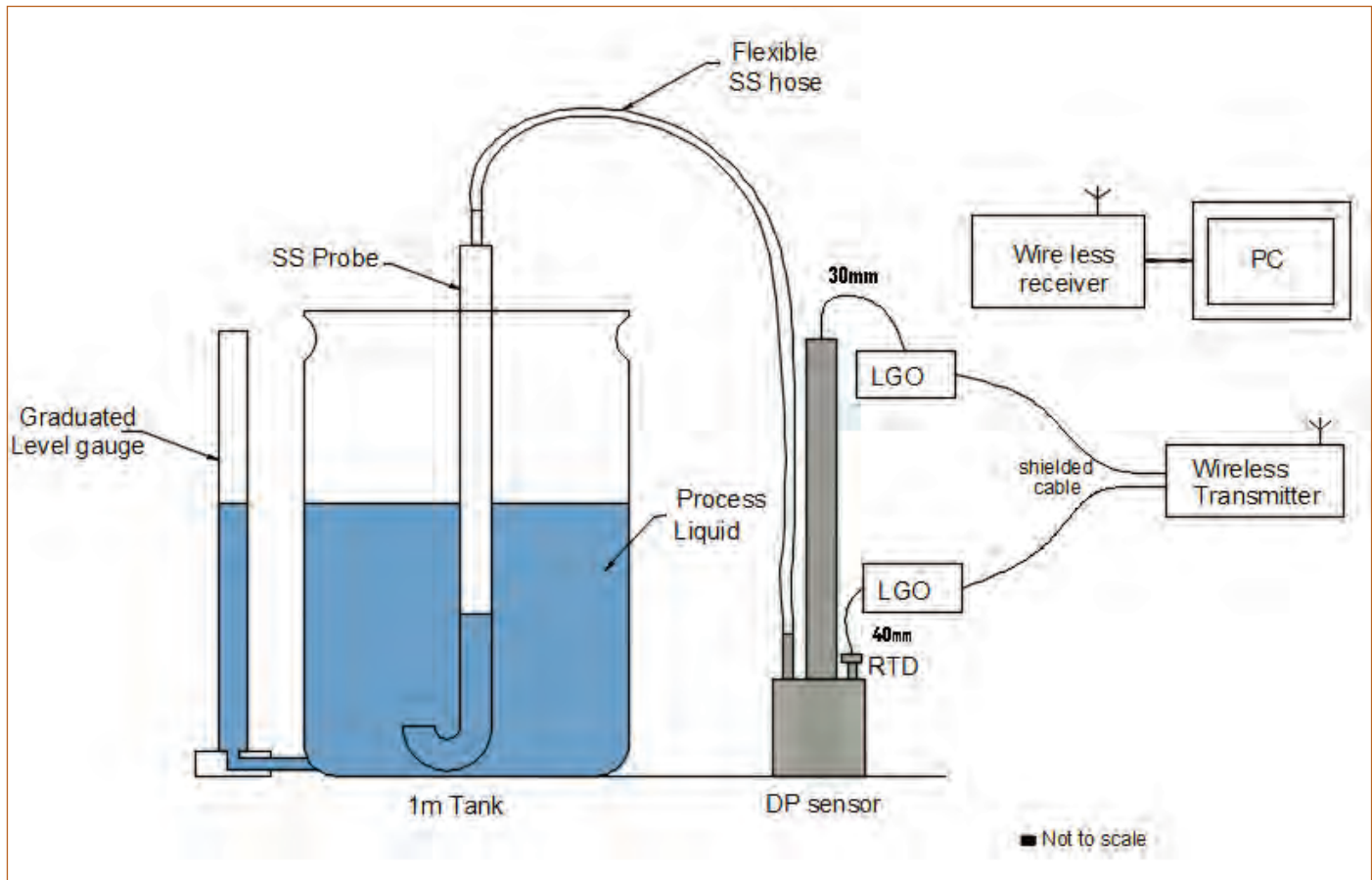


Figure 3: Level sensor arrangement

In this case the manometer limbs are of uniform diameter and hence

$$\partial\Delta h = \Delta V_{(appx)} / [(\pi/4)((\rho_o/\rho_w)*D^2) + (0.5 * d^2)] \quad (16)$$

The temperature compensated  $\Delta h$  ( $\Delta h_{comp}$ ) corresponding to water level  $H$  is given by

$$\Delta h_{comp} = \Delta h_2 - \partial\Delta h \quad (17)$$

Hence  $\Delta h_{comp}$  gives the information of actual liquid level in the tank irrespective of change in ambient temperature. This approximation method has helped to considerably reduce the error in measurement (from 5% to  $\sim 1\%$ ) due to change in ambient temperature.

### Differential Pressure Pulsating Sensor

Differential Pressure pulsating Sensor (DPS) is primarily a well type manometer. The primary signal of the sensor is in digital domain i.e. a train of rectangular pulses whose frequency determines the parameter being measured. Topology of DPS is shown Figure 2. The sensor assembly consists of two arms (A & B) made of two SS tubes widely differing in height and diameter. The tall and narrow tube (B) is placed inside the short and wide tube (A) with a common vertical axis. The sensing arm B is fabricated into rectangular cross section which provides room to accommodate six mirror finished stainless steel parallel plates. These electrodes constitute a floating type parallel plate capacitor

assembly. The arm A is partially filled with a fixed volume of low volatile mineral oil. As pressure is exerted through inlet of arm A, the oil rises through arm B, changing the capacitance of electrodes. Capacitors form a part of a RC Logic Gate Oscillator (LGO) whose resistance is fixed. Frequency output of LGO is inversely proportional to capacitance.

### Prototype LLM System

A prototype setup of 1 m liquid height for proposed technique of continuous LLM is constructed. A representative diagram is shown in Figure 3. The pressure exerted by liquid level at bottom of the container is measured by inserting a probe of diameter 1.5" vertically into the tank. The probe diameter is determined using Equation 2 considering the maximum resolution required for measurement. The bottom end of probe is made to a U-bend so that a minimum level of water level is maintained even though the tank is empty. This avoids, escape of trapped air when the tank is empty and helps to hold the calibration. The manometer is replaced by a high-resolution differential pressure pulsating sensor which measures the hydrostatic pressure with respect to atmospheric pressure. The probe is connected to DPS using flexible SS hose. Resistance Temperature Detector (RTD) is mounted on arm A of sensor to measure the trapped air temperature. RTD forms a part of another LGO whose capacitance is fixed. The complete assembly including probe, flexible hose



Figure 4: Level measurement system (a) DP Sensor, (b) probe inserted to tank, (c) wireless receiver and (d) wireless transmitter

and DPS is subjected to Helium Leak Test in order to ensure leak tight connections. The LGO output frequency is slightly affected by change in temperature, but it is found to be insignificant. Wireless transmitter calculates the temperature compensated level from the output of both LGOs and communicates to wireless receiver.

#### Calibration

LLM system requires a set of multi-point calibration before deployment. Frequency versus temperature calibration for RTD is carried out using constant temperature bath. Frequency vs  $\Delta h$  calibration of DPS is performed using a specific U-tube manometer setup. The above-mentioned calibrations are done at lab before deployment. The only calibration to be performed at field is Frequency versus Level. Graduated level gauge is used for this purpose. All the calibration data is plotted using least square fitting to obtain polynomial equations. The coefficients of equations are fed to wireless receiver unit which calculates level and temperature from the frequency output of LGOs and evaluate the temperature compensated level.

#### Performance Analysis

The calibrated prototype level measurement system for 1m range is subjected to performance tests. Based on the results of performance test, the salient features of level measurement system are listed below: (a) continuous type level sensor (b) suitable for use in any kind of liquid irrespective of chemical constituents, conducting or non-conducting (c) temperature compensated and tested up to 40°C (d) Range of application: 0–1 m. Same DP sensor can be used for different ranges by suitable modification in probe alone (e) no bubbling effect (f)

accuracy: ~1%, (g) precision in measurement: less than 1.1 mm (h) resolution: 3 mm, (i) hysteresis: <1%, (j) response time: 4s. Apart from above mentioned performance parameters, the system is also enhanced with industry requirements such as wireless data acquisition, integrated keypad for field calibration, 4–20 mA output at wireless receiver, potential free contacts for control and RS232 output for data logging.

#### Deployment of LLM system at Sewage Treatment Plant, Kalpakkam

The level measurement system is put to a real-world application; it is used to measure the level of sewage water buffer tank of Bioreactor situated at STP (Sewage Treatment Plant), Kalpakkam. The nature of sewage water caused frequent failure of conventional intrusive type of measurement systems. The advantages of LLM system such as top mountable, indirect measurement, continuous-type etc. made it suitable for this application.

A 1.7m range level measurement system is fabricated. Helium Leak test was carried out on system to confirm the leak tightness and performance is studied using test setup at WSCD bay. Snapshots of sub-modules of LLM system taken during testing is shown in Figure 4. After successful testing, the system is deployed at the field. The system is used to continuously monitor the level of buffer tank and control the pump to avoid overflow and emptying of the tank. The performance was monitored for a period of 2 months and found to be satisfactory.

*K. Praveen and colleagues  
Electronics & Instrumentation Group*

## Young Officer's FORUM

### Multiferroicity Induced in $GdMnO_3$ by 30% Y Substitution

Materials exhibiting more than one long range ordered ferroic property (magnetic, electric and strain) in their single phase are called multiferroic. Among these, materials possessing simultaneous electric and magnetic order with a strong coupling between them are of special interest, as these materials would widen the horizon of applications as one of the ferroic properties could control/modify another; especially control of magnetic property on application of external electric field. These materials are broadly classified as type I and type II multiferroics based on their electric and magnetic coupling strength. Type I multiferroic systems have different origin for their electric and magnetic ordering and the coupling between them is weak. These systems also have a large difference in their electric and magnetic ordering temperatures.  $BiFeO_3$  and  $BiMnO_3$  belong to this category. On the other hand, type II systems have strong coupling between their ferroic orders. Interestingly, ferroelectric ordering in this system is not by structural symmetry changes as seen in conventional ferroelectric system but by magnetic transition leading to spontaneous polarization.  $TbMnO_3$  is the best studied type II multiferroic system. Because of the coupling between the ferroic properties, polarization direction can be changed by changing the

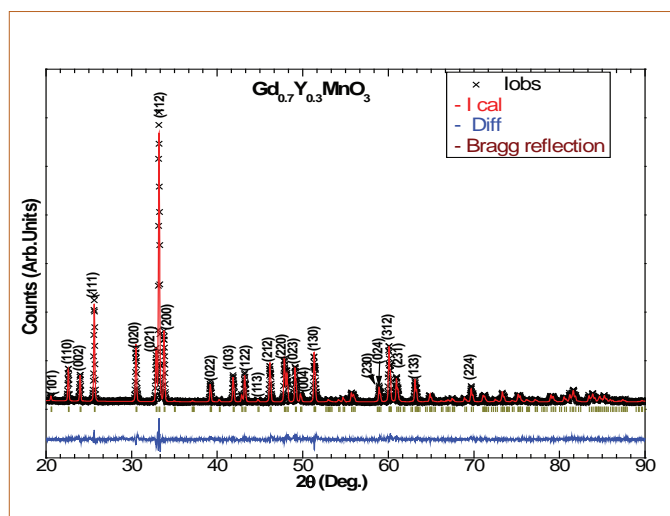


Figure 1: XRD pattern of  $Gd_{0.7}Y_{0.3}MnO_3$  at room temperature



Dr. R. M. Sarguna joined X-rays & Crystal Growth Section, Materials Science Group, Indira Gandhi Centre for Atomic Research in the year 2005 after completing OCES from 5<sup>th</sup> batch of RRCAT training school. He obtained his M.Sc. from University of Madras, Chennai in 2004 and Ph.D from HBNI in the year 2014. Current area of work comprises structural and dielectric studies of functional materials.

direction of the applied magnetic field.

Rare earth manganite  $RMnO_3$  (R: rare earth ion) with orthorhombic Perovskite structure have the attribute that their crystal structure and hence their magnetic structure can be changed by varying the rare earth ionic radius. This tunability gives the advantage of inducing multiferroic property even in those which are otherwise non multiferroic. For  $RMnO_3$  systems to show multiferroic property they should have long wavelength modulated magnetic structure incommensurate with that of crystal lattice. This happens only over a narrow window range of rare earth ionic radius (eg. Tb-Dy). For few others this can be brought in by partially substituting R site with other rare earth ions of suitable ionic radii. Towards this we have substituted Yttrium ( $Y^{3+}$ ) at Gadolinium ( $Gd^{3+}$ ) site in  $GdMnO_3$  to induce multiferroic property in its ground state. The multiferroic property in these systems is attributed to the spin-lattice coupling where the ferroelectricity arises due to lattice distortion caused by magnetic structure as explained by inverse Dzyaloshinskii-Moriya interaction.

Here we report studies on inducing ferroelectric property in an otherwise paraelectric and antiferromagnetic  $GdMnO_3$  by 30 at.% substitution of  $Gd^{3+}$  with  $Y^{3+}$ . Substitution results in requisite

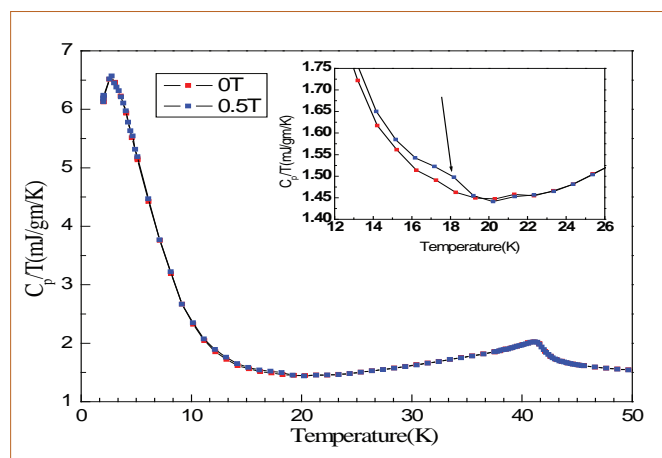


Figure 2:  $C_p/T$  versus  $T$  plot for  $Gd_{0.7}Y_{0.3}MnO_3$  under an applied magnetic field of 0 and 0.5 T. Inset shows expanded view of the same plot in the temperature interval 12 to 26K

structural modification to observe ferroelectric property. The magnetic, dielectric and structural studies in the temperature interval 5 to 70 K were carried out employing thermomagnetization, specific heat, broad band impedance spectroscopy and synchrotron based powder X-ray diffraction (XRD) respectively.

The XRD pattern of  $Gd_{0.7}Y_{0.3}MnO_3$  system shown in Figure 1 could be indexed to orthorhombic symmetry belonging to Pbnm space group. Upon Y substitution, the lattice parameters contract anisotropically with respect to the parent  $GdMnO_3$ . However, the relation  $c/\sqrt{2} < a < b$  corresponding to  $O'$  distortion of the orthoPerovskite is obeyed. Observed decrease in the lattice parameters is in accordance with the smaller ionic radius of  $Y^{3+}$  (1.075 Å) compared to that  $Gd^{3+}$  (1.107 Å). Also, estimated average Mn-O-Mn bond angle is reduced from  $146.1^\circ$  (for  $GdMnO_3$ ) to  $\sim 144.8^\circ$  and fall in the window range that is amenable for observation of multiferroic property.

From thermomagnetization studies, the susceptibility is seen to monotonically increase (not shown) with lowering of temperature. Absence of signature for magnetic transitions is attributed to the substantial paramagnetic contribution of  $Gd^{3+}$  sublattice close to the expected para to antiferromagnetic (AFM) transition temperature ( $\sim 40$  K) of the  $Mn^{3+}$  sublattice. Nonetheless, from the Curie-Weiss analysis of the thermomagnetization data, antiferromagnetic interaction between the moments is clearly established. In order to determine the magnetic transition temperatures associated with  $Gd^{3+}$  and  $Mn^{3+}$  sublattices, specific heat measurements were carried out. A  $C_p/T$  versus T plot is shown in Figure 2. A  $\lambda$ -like anomaly, characteristic of AFM transition could be observed at about 41 K. It is attributed to AFM transition of  $Mn^{3+}$  sublattice having an

incommensurate sinusoidal magnetic structure. This is about 2 K lower compared to that of  $GdMnO_3$ . On the other hand, AFM transition temperature of  $Gd^{3+}$  sublattice, seen as a prominent anomaly about 7 K is not affected by  $Y^{3+}$  substitution. This clearly indicates that structural effects are predominant compared to dilution effects in weakening the magnetic transition interaction. In addition to these a weak but definite anomaly is observed about 18 K. Strength of this anomaly marginally increases upon application of magnetic field. This indicates that the origin of this anomaly lays at a subtle change in the magnetic structure of  $Mn^{3+}$  sublattice.

Temperature dependence of the real  $\epsilon'(T)$  and imaginary  $\epsilon''(T)$  parts of permittivity of  $Gd_{0.7}Y_{0.3}MnO_3$  measured at different frequencies are shown in Figure 3. Both  $\epsilon'(T)$  and  $\epsilon''(T)$  exhibit for all frequencies, an anomaly in the form of a peak centered about 17 K with a weak shoulder about 7 K. The weak shoulder corresponds to AFM transition of  $Gd^{3+}$ -sublattice. It is interesting to note that magnetic transition of the  $Gd^{3+}$ -sublattice contributes to dielectric properties of the system. For the parent compound  $GdMnO_3$  a step like anomaly has been reported and is ascribed a metamagnetic transition at which the modulation propagation wave vector of  $Mn^{3+}$  sublattice abruptly drops from a finite value to zero. Such a transition is shown to leave the ground state of  $GdMnO_3$  to be paraelectric. However, the ground state modifies to ferroelectric in the presence of external magnetic field and step like a feature in the dielectric response modifies to a peak with concurrent appearance of induced ferroelectric phase transition. Thus, a peak in the dielectric response, instead of step like feature in the present compound indicates induced ferroelectric phase transition. Thus it is inferred that Y substitution is able to induce spontaneous ferroelectric order in  $GdMnO_3$ , which otherwise

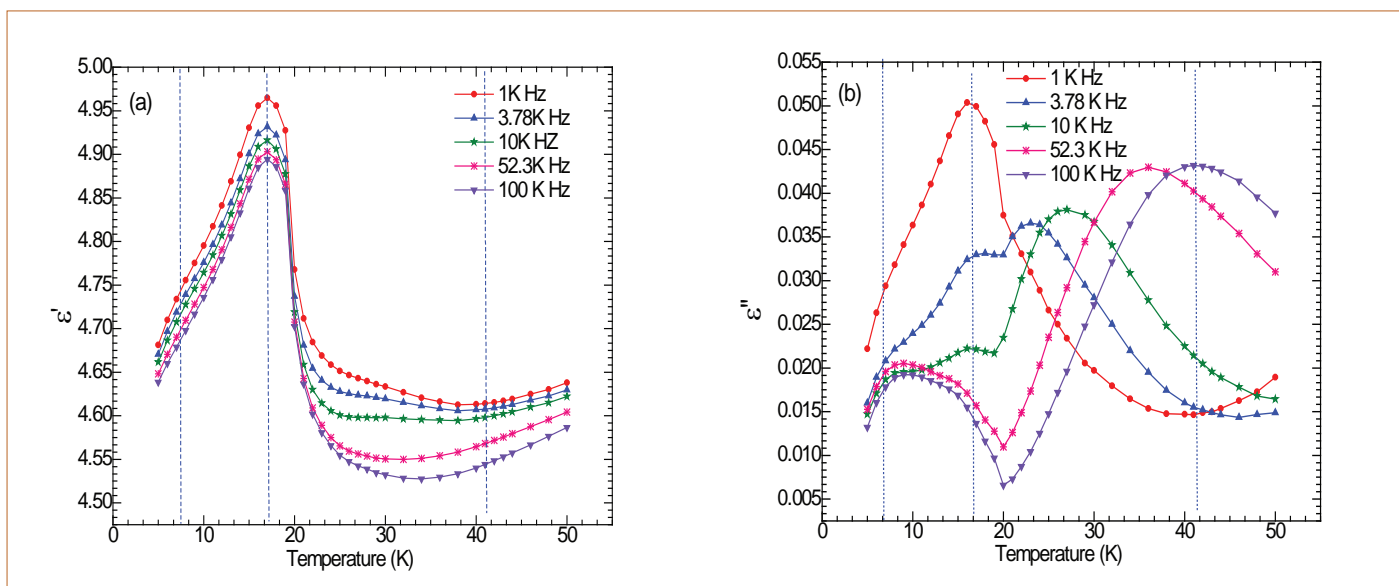


Figure 3: Temperature dependence of (a) real and (b) imaginary part of dielectric constant of  $Gd_{0.7}Y_{0.3}MnO_3$  measured under different frequencies

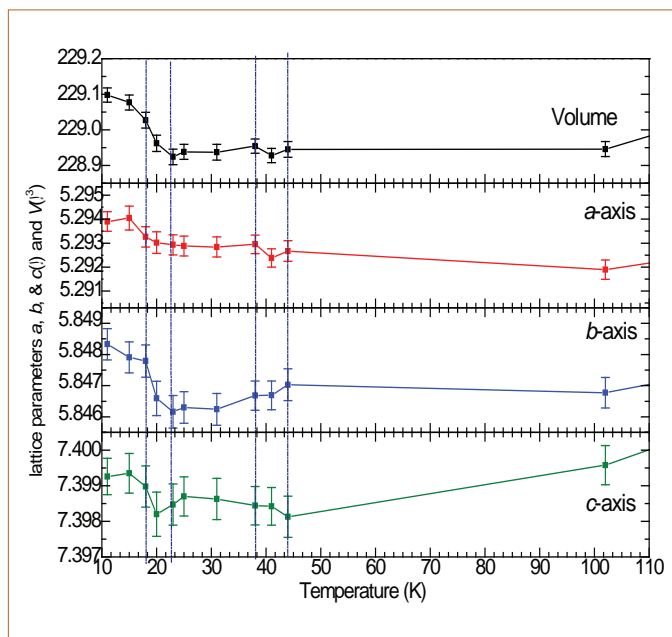


Figure 4: Temperature dependent lattice parameter variation of  $Gd_{0.7}Y_{0.3}MnO_3$

has to be induced by external magnetic field. Interestingly, no anomaly associated AFM transition of  $Mn^{3+}$  sublattice is observed. It is clearly seen that while the position of anomaly in associated with FM and AFM of  $Gd^{3+}$  sublattice are almost independent of frequency, strength is found to dramatically decrease with frequency about the temperature region covering these transitions. In addition to these anomalies, additional broader anomaly evolves with frequency; position of which shifts to higher temperature with increased strength with frequency. The anticorrelation of strength of the anomalies of these processes with frequency clearly indicates that process associated with broad anomaly is different from that associated with FE. As mentioned above featureless behavior of  $\chi(T)$  along with frequency-dispersive  $\chi(T)$  indicates a conductive behavior associated with thermally-activated relaxation and is called as para-process.

Variations of the lattice parameters  $a$ ,  $b$ ,  $c$  and unit cell volume  $v$  in the temperature interval 0 to 50 K was studied using angle dispersive XRD technique at beam line (BL-12) of Indus-2 synchrotron. The lattice parameters exhibit anomalous variations in their temperature dependence about the magnetic transitions AFM and induced ferroelectric (FE) transition temperatures. It is seen that  $a$ -axis exhibits negative thermal expansion with a dip about 41K and steep increase about 20K. Though  $b$ -axis also registers a steep increase about 20K, it exhibits positive thermal expansion between the magnetic transition AFM and FE temperature. On the other hand,  $c$ -axis in the same temperature range is almost temperature independent, followed by a steep raise about 20K. It is pertinent to note that all the lattice parameters steeply rise across the FE transition temperature.

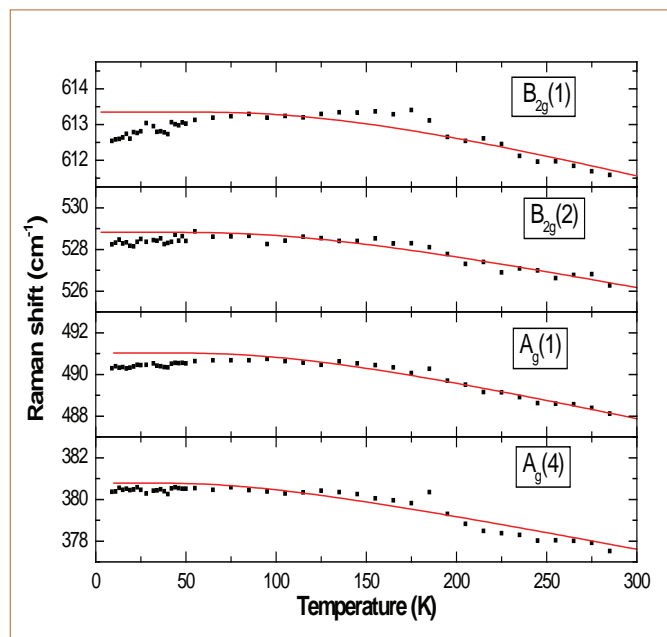


Figure 5: Raman peak shift as a function of temperature. Red curve shows fitting of anharmonic behavior

This feature may be associated with large magnetoelastic effect in this compound.

The magnetic and crystallographic changes are expected to have strong correlation with the underlying lattice phonons. The shift in phonon modes across the magnetic transition has been attributed to spin-phonon coupling. Presence of spin-phonon coupling is one of the necessary but not sufficient conditions for a material to be multiferroic. Raman spectroscopy has been used to study the phonon modes from room temperature down till 10K in  $Gd_{0.7}Y_{0.3}MnO_3$  to ascertain the presence of spin-phonon coupling and hence its multiferroic nature. Anharmonicity of the lattice force constant is prime factor responsible for shift in phonon frequency with temperature in insulating magnetic systems. Any deviation from this variation is attributed to presence of spin-phonon coupling. Among all the modes the  $B_{2g}(1)$  mode belonging to the in-plane stretching of the oxygen in the  $MnO_6$  octahedra is observed to show maximum deviation. This is shown in Figure 5 by fitting the anharmonic contribution as a function of temperature to phonon shift. The variation of FWHM of the Raman peaks gives an idea of life time of the relaxation. This has also been studied as a function of temperature and has been shown to have additional relaxation in the form of spin-phonon coupling. These studies confirm the presence of spin phonon coupling and hence the multiferroic nature of Y substituted  $GdMnO_3$ .

*R. M. Sarguna and colleagues  
Materials Science Group*



## Young Researcher's FORUM

### Light-Matter Interaction of Sub-diffraction Limited Nanostructures

The optical characterization of semiconductor nanostructures is described as the study of the interaction between materials with the photon of the electromagnetic (EM) radiations. The light-matter interaction at the near-field regime of nanostructures is a very interesting as well as challenging task in the scientific community. For a wavelength  $\lambda$ , the Abbe's diffraction limit prevents conventional optical microscopes to possess a spatial resolution beyond the value of  $\sim\lambda/2$ , even for a maximum numerical aperture (unity) of the probing objective. The near-field scanning optical microscopy (NSOM) assisted with the help of plasmonics is a unique tool to understand the light-matter interaction in the sub-diffraction limit. The evanescent field emanating from the NSOM probe with higher momenta (i.e.; lower wavelength and velocity) compared to that of the normal light is not diffraction limited. Hence, it facilitates optical and spectroscopic imaging of objects with nanometer scale spatial resolution. In addition to that, the rate of interaction of a material with EM radiation can also be enhanced by keeping it in a micro-cavity. The proximity induced long lived interactive photons, enhances the photon density leading to the increase in emission/absorption of light.

Using the far-field imaging technique, we have recorded polarized spectroscopic photoluminescence (PL) imaging of a single AlGaIn nanowire (NW) of diameter  $\sim 110$  nm using proximity induced confinement of light with  $l=325$  nm. We also investigated the light-matter interaction of an isolated single AlGaIn NW in the near-field regime by using the NSOM technique using  $l=532$  nm.

#### The proximity induced optical confinement

The field emission scanning electron microscopy (FESEM; SUPRA 55 Zeiss) image (Figure 1) shows the uniform and mono-dispersed NWs all over the substrate with a narrow size distribution of  $100 (\pm 10)$  nm (Figure 1b). The high resolution image (outset of Figure 1b) of the cylindrically shaped AlGaIn NWs shows very smooth surface morphology with an Au nanoparticle (NP) at the tip



Dr. A. K. Sivadasan obtained his M.Sc. in physics from Sri Vyasa N.S.S College, Calicut University, Kerala. He joined as a research fellow in 2012 to pursue his doctorate under the guidance of Dr. Sandip Dhara. His current area of interest is to investigate the optical properties of group III nitride nanostructures using far-field and near-field spectroscopic techniques. He obtained his Ph.D. thesis in 2016 from Homi Bhabha National Institute (HBNI).

( $\sim 120$  nm) along with well separated NPs. The polarized PL measurements at 300K for the single AlGaIn NW are performed with the help of the Raman spectrometer (in Via, Renishaw, UK) in two different configurations of  $Z(XX)\bar{Z}$  and  $Z(XY)\bar{Z}$ , which are considered as parallel ( $\pi$ ) and perpendicular ( $\sigma$ ) polarizations, respectively. In the Porto notations, the first and last letters, represent the direction of the propagation of the incident (Z) and backscattered wave vectors ( $\bar{Z}$ ), respectively. Similarly, the second and third letters inside the parenthesis represents the direction of the electric field polarization of the incident ( $E_i$ ) and scattered light ( $E_s$ ), respectively. The parallel  $Z(XX)\bar{Z}$  and perpendicular  $Z(XY)\bar{Z}$  polarization was configured using a half wave plate and a polarizer kept in the backscattering geometry.

It was found that the polarized PL peak intensity for a single NW is higher for  $\pi$ -polarization, as compared to that of the  $\sigma$ -polarization (Figures 1c and 1d). The optical image of the mono-dispersed AlGaIn NW used for recording the PL spectra is indicated by a dotted arrow in Figure 1c. It was ensured that the individual NWs were well separated ( $\sim 2 \mu\text{m}$ ) compared to the excitation laser spot size of  $\sim 0.8 \mu\text{m}$  to receive a PL spectrum of a single NW alone. The PL emission at  $\sim 3.53$  eV is reported to originate because of the electron ( $e^-$ )-hole recombination of free exciton (FE). A tiny peak centered at 3.73 eV is assigned to A1(LO) mode of GaIn. The peak observed at  $\sim 3.30$  eV is identified as the donor acceptor pair (DAP) transition from a shallow donor state of nitrogen vacancy (VN) to a deep acceptor state of Ga vacancy (VGa). The variation in intensity for different polarization configurations depends on the material geometry as well as the anisotropy of the medium. Thus, the intensity of  $\pi$ -polarization ( $I_\pi$ ) can be different from that of  $\sigma$ -polarization ( $I_\sigma$ ) due to the confinement effect originated because of the dielectric contrast of NWs and surrounding media. For the present study, the polarization ratio PL emission ( $r=I_\pi/I_\sigma+I_\sigma$ ) for the AlGaIn NW was calculated as  $\sim 0.533$ .

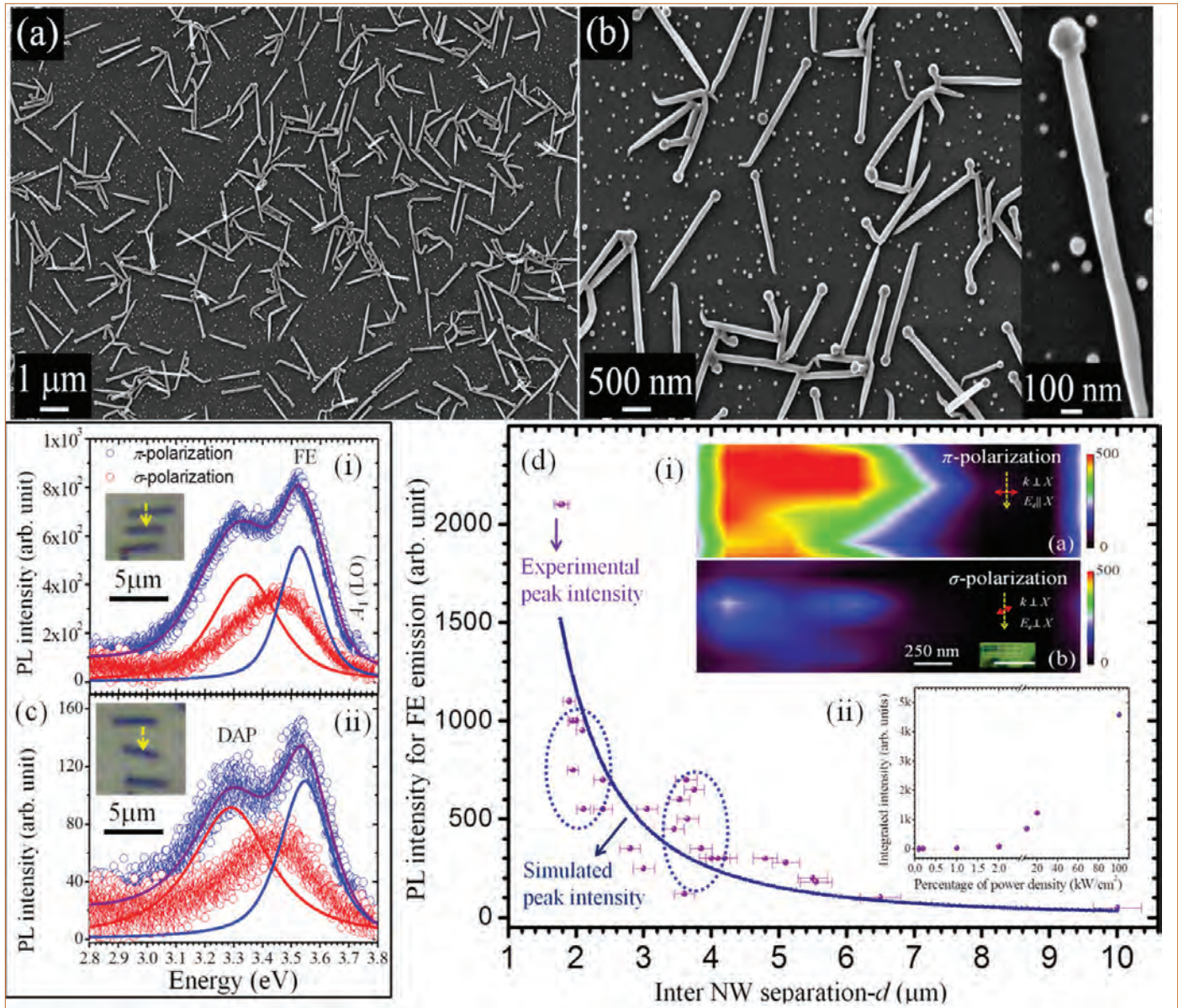


Figure 1: Morphology of AlGaN NWs (a) low and (b) high magnification images with a single NW shown in the inset. (c) Polarized PL spectra for  $\pi$ - and  $\sigma$ -polarized configurations of a single AlGaN NW (indicated by an arrow in the inset optical images) for  $d =$  (i)  $2 \mu\text{m}$  and (ii)  $4 \mu\text{m}$ . (d) The statistical dependence of FE emission with respect to the  $d$ . Insets (i) (a)  $\pi$ - and (b)  $\sigma$ -polarized PL maps for a single AlGaN NW. The optical image of a typical single NW with a schematic grid pattern used for PL imaging is shown in the inset. The scale bar corresponds to a length of  $3 \mu\text{m}$ . Inset (ii) the integrated peak intensity vs. PD from a single NW with  $d \sim 2 \mu\text{m}$

A strong correlation of the PL intensity ( $I_{PL}$ ) (Figures 1c(i) and 1c(ii)) with the proximity to other NWs was observed in the present study. An increase in  $I_{PL}$  by one order is observed, when the inter-NW separation ( $d$ ) is decreased from  $4 \mu\text{m}$  (inset Figure 1c(i)) to  $2 \mu\text{m}$  (inset Figure 1c(ii)). The similar experiments were carried out for several times with different  $d$  to get a good statistics (Figure 1d). Interestingly, the  $I_{PL}$  varies inversely proportional the interaction area ( $l \times d$ ), where  $l$  is the length of NW (Figure 1d). However, the scattering of the data-points observed for the  $I_{PL}$  with respect to  $d$  is possibly because of the misalignment of NWs from its perfect parallel configuration with each other (as indicated by the error bars for the x-scale in Figure 1d).

A collection of AlGaN NWs with close proximity to each other, may lead to the existence of reasonably long lived photons (owing to multiple interactions and excitonic transitions) in the intervening space between the NWs. These localized photons exist in between the intervening space of NWs as long as the external pump laser is on. A nonzero non-equilibrium population density of such photons increases the stimulated emission by utilizing  $e$ -s in excited states. The quantitative analysis of the phenomenon leads to an expression for the emission  $I_{PL}$ ,

$$I_{PL} \propto \mu R_P \tau_{sp} (1 + 2\sigma V_g N \tau_{ph} / V) \dots \dots \dots (1)$$

Where,  $R_P$  is the rate at which  $e$ -s are pumped to an excited state by

absorption of photons,  $\sigma$  is the cross sectional area for stimulated emission caused by a single  $e^-$ ,  $\tau_{ph}$  is the lifetime of localized long lived photons, and  $N$  be the total number of photons. Moreover, the second term in the equation (1) is responsible for the increase in  $I_{PL}$  due to the presence of the intervening long lived photons in between the NWs. Therefore, the PL intensity is inversely proportional to the available interaction volume ( $V$ ) occupied by these photons. Since,  $V = h \times l \times d$  where,  $h$  is the height of NW. So, for a fixed  $h$  ( $\sim 100$  nm), the increase in PL intensity is inversely proportional to the interaction area ( $l \times d$ ).

The PL imaging of single AlGaIn NW with an average diameter  $100 (\pm 10)$  nm is carried out over an area of  $3 \times 1 \mu\text{m}^2$  using an excitation laser of wavelength of 325 nm. The Figure 1d(i) shows the PL maps of single NW generated by integrating the intensity of FE emission for  $\pi$ - and  $\sigma$ -polarization (Figure 1d(i(a) and i(b)). The optical image of a single NW used for PL maps are also shown (inset Figure 1d(i(b))) with a schematic grid pattern. The scale bar of  $3 \mu\text{m}$  represents the true dimension along the long axis of the NW only. The variation of IPL in the maps observed for different polarization configuration is due to the difference in the interaction of electric field strength with NW. In  $\pi$ -polarization, the excitation electric field which is parallel to the NW long axis strongly interacts with the NW (Figure 1d(i(a))). In this configuration, the magnitude of interacting electric field  $E_{i\pi}$  in the NW medium remains same as the excitation electric field  $E_{e\pi}$  (ie;  $E_{i\pi} \sim E_{e\pi}$ ). Whereas, in case of  $\sigma$ -polarization, the internal electric field  $E_{i\sigma}$  will attenuate according to the relation  $E_{i\sigma} = [2\varepsilon_0 / (\varepsilon + \varepsilon_0)]E_{e\sigma}$ , where  $E_{e\sigma}$  is the external electric field perpendicular to the long axis,  $\varepsilon$  is the dielectric constant of the NW ( $\sim 5.8$  for GaN) and  $\varepsilon_0 = 1$  in air or vacuum. PL maps for FE emissions with different polarizations (Figure 1d(i(a) and i(b)) are observed to be good agreement with the above relation. Moreover, the excitation laser (pump) power dependence of emission from a single NW with  $d \sim 2 \mu\text{m}$  is also investigated. The integrated emission peak intensity vs. excitation laser power density (PD) (Figure 1d(ii)) shows a linear behaviour after threshold, which is a confirmation for the possible presence of stimulated emission process. In the Abbe's diffraction limit ( $\lambda/2N.A.$ ), the far field spectroscopic imaging or focusing is not possible for nanostructures having dimension  $< 325$  nm while using 325 nm excitation wavelength and an objective lens with N.A. value of 0.50. However, the optical confinement effect for the light-matter interaction allows one to record the PL maps of single AlGaIn NW in the sub-wavelength scale even in the absence of any plasmonic effect. The dimension of PL maps of single NW ( $\sim 200$  nm) using  $\pi$ -polarization is found to be enlarged as compared to the FESEM images of a single AlGaIn NW ( $\sim 100$  nm; outset Figure 1b). The spread is essentially due to the focusing limit ( $\sim 0.8 \mu\text{m}$ ) of the incident beam which is higher than the spatial resolution ( $\sim 100$  nm) of the motorized sample stage used for the PL mapping.

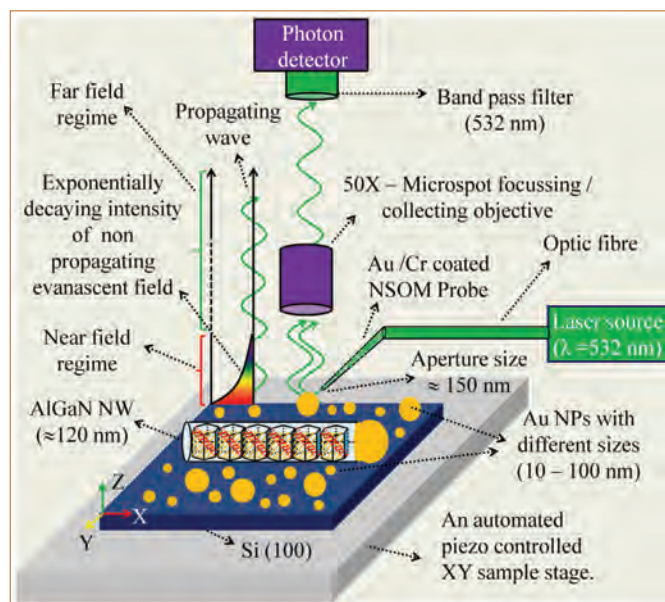


Figure 2: The schematic experimental setup for NSOM imaging of AlGaIn NW and Au NPs with the near field excitation and far field collection configuration

### Near field interactions of visible light with sub-diffraction limited nanostructures

The schematic of experimental set up (MultiView 4000; Nanonics, Israel) of the NSOM is shown in the Figure 2 used for the imaging of semiconductor AlGaIn NW and metallic Au NP. The interaction of 532 nm laser ( $\sim 2.33$  eV) with NW and NPs were studied using an atomic force microscopic (AFM) probe for simultaneous scanning of the topography with the tuning fork feedback mechanism. A band pass filter (532 nm) was used to extract the photons after the light-matter interaction and before reaching to the detector in the far field configuration.

The resultant near field light-matter interaction is shown for AlGaIn single NW along with Au NPs of various sizes (Figure 3) The high resolution topographic AFM image of the single NW in the two-dimension (2D) and 3D (Figures 3a and 3b) shows smooth and cylindrical shape, as observed in the FESEM images, with a diameter of  $\sim 120$  nm. The height variations of AFM cantilever along the line across Au NP-AlGaIn NW-Au NP shows (Figure 3c) the height of AlGaIn NW and Au NP as 120 and 40 nm, respectively. Moreover, we also observed Au NPs with a size smaller than 40 nm in the same image and it was very clearly resolved by the NSOM technique with an aperture probe diameter of 150 nm. The Au NPs with a size  $\sim 20$  nm is encircled in the AFM topography (Figure 3a) and in the optically resolved NSOM (Figure 3b) images. The NSOM images of AlGaIn single NW as well as catalyst Au NPs in 2D and 3D are shown in Figures 3d and 3e. Since, the diameter of AlGaIn NW ( $\sim 120$  nm) is far below the diffraction limit, one need to shorten the wavelength down to the sub-diffraction regime for obtaining highly resolved optical images. Using metal coated NSOM probe,

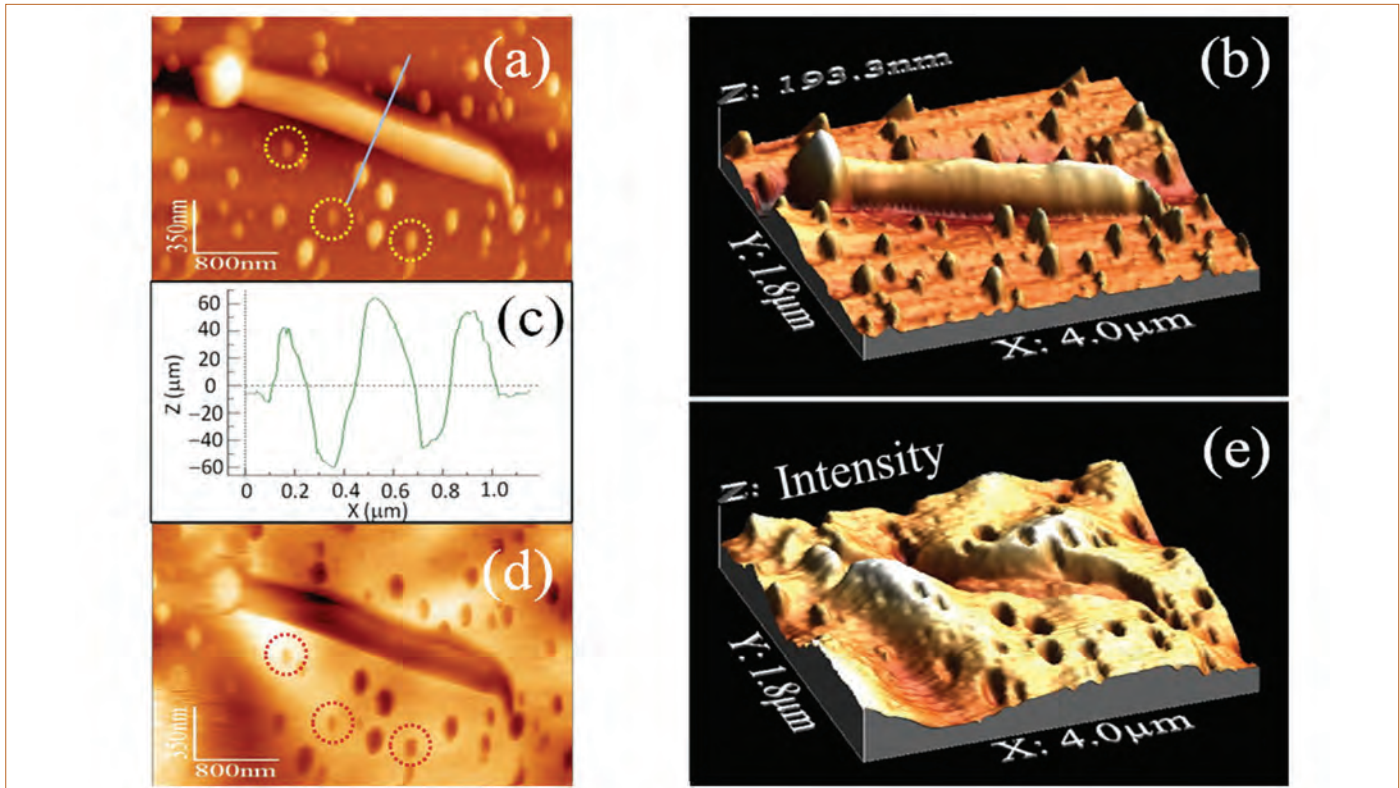


Figure 3: The topographic (a) 2D (b) 3D AFM images of a single AlGaIn NW along with Au NPs, (c) The height variation of AFM cantilever along the line across Au NP-AlGaIn NW-Au NP as shown in (a) and the corresponding (d) 2D and (e) 3D optical NSOM images. Au NPs with size  $\sim 20$  nm is encircled in the AFM topography and in the optically resolved NSOM images

it is possible to produce an evanescent wave with momentum higher than that of the original excitation wavelength  $\lambda_0 = 2\pi/k_0(\omega)$  with wave vector of  $k_0(\omega) = \omega/c$ , where  $c$  is the velocity of light. Therefore, the evanescent waves emanating from the NSOM probe aperture possess a group of wave vectors higher than that of the original excitation laser as  $k_{ev}(\omega) = \omega/v$ , with different velocities ( $v$ ) slower than the excitation wave velocity ( $v < c$ ).

Thus, the NSOM offers the possibility of optical as well as spectroscopic imaging in the sub-diffraction regime with super-resolution. At the same time, it preserves the excitation frequency and energy. By taking this advantage, we used the NSOM technique to understand the interaction of green laser (532 nm = 2.33 eV) with single semiconductor AlGaIn NW in the near-field regime. Furthermore, in the present study, we have achieved an optical special resolution up to the order of  $\sim 20$  nm with the 150 nm aperture probe. The reported RT band gap of AlGaIn NWs is 3.53 eV, which is higher than the excitation energy of 2.33 eV. Therefore, a complete transmission of light through the AlGaIn NW is expected. Surprisingly, however we observed a prominent absorption of light along the AlGaIn NW, as shown in the NSOM images in 2D and 3D (Figures 3d and 3e). The interaction of single AlGaIn NW with light in the near-field regime is realized by using the help of possible energy levels related to native defect states. The excitation energy of 2.33 eV is sufficient to activate the transitions corresponding to emission energies  $\sim 2.05$  and  $\sim 1.76$  eV

(reported for AlGaIn samples) by the absorption of photons. The emissions at  $\sim 1.76$  and  $\sim 2.05$  eV are blocked by the band pass filter used before the detector in the NSOM experimental setup (Figure 2). Therefore, the probing light energy is utilized for exciting the defect levels and hence we observe a significant absorption along the single NW in the NSOM images (Figures 3d and 3e). In the NSOM images, we also observed strong surface plasmon resonance related absorption for Au NPs.

In summary, we have recorded the far-field spectroscopic image using the polarized PL spectra for a single AlGaIn NW with a diameter 100 ( $\pm 10$ ) nm in the sub-wavelength scale. A nonzero non-equilibrium population of such photons may cause additional stimulated emission, leading to enhanced PL emission. We envisage the use of the NSOM technique for direct understanding of light-matter interaction of semiconductor as well as metallic nanostructures of sub-diffraction limited dimension in the near field regime. As a major accomplishment, we achieved an optical spatial resolution up to  $\sim 20$  nm even with a 150 nm apertured NSOM probe. The isolated single and semiconductor AlGaIn NW with a diameter  $\sim 120$  nm shows a strong absorption of visible light due to the electronic transitions originated from the native defect related energy levels.

A. K. Sivadasan  
Materials Science Group

## Conference and Meeting Highlights

### 13<sup>th</sup> CEA-IGCAR Annual Meeting on LMFBR Safety

October 03-06, 2017



CEA and DAE delegates during the meeting

DAE and CEA, France have been working together in the field of liquid metal fast breeder safety collaborative project. 13<sup>th</sup> CEA-IGCAR annual meeting to review ongoing collaborative projects was held during October 3-6, 2017. DAE team was led by Dr. Arun Kumar Bhaduri, Director, IGCAR and CEA team consisting of 11 experts was led by Dr. Christian Latge. During the meeting few new implementing agreements for collaboration on new projects were discussed. Meetings were divided into six sessions for discussion on topics namely Instrumentation, status of ongoing Implementing Agreement (IA), new topics for Potential Collaboration, Severe Accident, Sodium Aerosol Behavior and Plenary Session. In the Plenary Session status of PFBR, FBTR and ongoing R&D for FBR were presented. Visits to PFBR, FBTR and other experimental facility were arranged for CEA delegates. The collaborative projects were reviewed during the meeting and the projects which were completed were closed.

*B. K. Nashine  
Indian Coordinator, CEA-IGCAR Collaborative Project*

## News and Events

### India International Science Festival 2017 - Kalam Science Yatra

October 13-16, 2017

As forerunner to India International Science Festival (IISF), (held at Chennai during October 13-16, 2017) a Science Yatra to spread the awareness about the event as well about Nuclear energy was organized. Department of Atomic Energy has identified IGCAR as one of its participants for IISF. IGCAR under the guidance of Dr. Arun Kumar Bhaduri, Director, IGCAR, took the responsibility of organizing the Yatra in the southern part of Tamil Nadu. The Science Yatra started off, aptly from Rameswaram, the birth place of our late president Bharat Ratna Dr. A.P.J. Abdul Kalam. A small function was held at A.P.J. Abdul Kalam memorial Centre on October 4, 2017, wherein Shri Sheikh Salim Grand Nephew of Dr. A.P.J. Abdul Kalam, team of Scientists from IGCAR, led by



Science Yatra being flagged from Dr. Abdul Kalam Memorial Centre, Rameswaram

Dr. B. Venkatraman, Director, HSEG and RM&PAG, IGCAR, school students, teachers and local people participated in the event. The Science Yatra, appropriately named as Dr. Abdul Kalam- IISF Science Yatra, with the lead vehicle portraying the bust of Dr. A.P.J. Abdul Kalam, followed by a mobile Science lab - van from M/s Agastya foundations, Bengaluru, holding Science demonstration exhibits, depicting photographs of eminent Indian Scientists, radiation monitoring detectors and equipments and information about the IISF, was flagged off by Shri Sheikh Salim. The main objective of the yatra organised by DAE, IGCAR was to enlighten students on the benefits of Science and Technology to the society through lectures, demonstration experiments on science and radioactivity, quiz competitions and exhibitions displaying the posters and models about various aspects of DAE's program. The lectures and other discussions were held both in Tamil and English.

Starting from Dr. Kalam's memorial, the yatra stopped enroute at ten nodal institutions namely (i) Syed Ammal Arts and Science College, Ramanathapuram, (ii) Aditanar College, Tiruchendur, (iii) Kamaraj college for Arts & Science, Tuticorin (iv) Spic higher secondary school, Tuticorin, (v) Scott Christian college, Nagercoil (vi) PSN College, Tirunelveli, (vii) National Engineering College, Kovilpatti, (viii) Thiagarajar College, Madurai, (ix) Gandhigram Rural Institute, Dindigul and (x) SSN College, Kalavakkam, Chennai before finally arriving at Anna University. A four hour lecture cum demonstration program was organized at each of the nodal institution which coordinated in their respective areas with the neighbouring colleges and schools, ensuring maximum student and faculty participation. The lectures, exhibition and experiments were attended by more than about 5,000 students, faculty and public. The team members of science yatra led by Dr. B.Venkatraman, Director Health Safety and Environment Group included Dr. T. S. Lakshminarasimhan, Associate Director, RMG, Dr. R.Baskaran, Head, RSD, Smt. Jalaja Madan Mohan Head, TC&PAS, Dr. K. Sivasubramaniam, Head, RAMS, Shri S. Chandrasekhar, Dr. R. Sarangapani, Shri S. Balasundarm, Shri Alagu Raja, Shri Ramar, Dr. K. A. Venkatesan, Dr. R. Kumaresan, Shri Ramu and Shri Parthiban and they covered a total distance of approximately 1055 kms. The Science Yatra reached its logical destination - Anna University, Chennai where Dr. Abdul Kalam had his last official career, and was received by the university officials and enthusiastic students.

*B. Venkatraman*  
*Director, Health Safety and Environment Group*  
*& Resource Management and Public Awareness Group*

## Conference and Meeting Highlights

### National Conference on Condition Monitoring (NCCM-2017)

October 26-27, 2017



Dr. Arun Kumar Bhaduri, Director, IGCAR released the souvenir of NCCM-2017. (L-R) Dr. B. P. C. Rao, Convener, NCCM-2017, Dr. Arun Kumar Bhaduri, Director, IGCAR, Dr. V. Bhujanga Rao, President, CMSI, Dr. P. V. S. Ganesh Kumar, Senior Vice-President, CMSI

IGCAR and Condition Monitoring Society of India (CMSI) jointly organized the National Conference on Condition Monitoring (NCCM-2017) in Kalpakkam during October 26-27, 2017 with an objective to bring together professionals from industry, research and academics to discuss the advances in condition monitoring of rotating equipment, machinery and other plant components. Dr. Arun Kumar Bhaduri, Director, IGCAR, Kalpakkam inaugurated the conference on 26<sup>th</sup> October and addressed the delegates. He highlighted the need for implementing proactive condition monitoring programs using vibration, thermography, acoustic emission and other techniques. He released a book on 'Condition Monitoring' by Prof. V. Ramamurthi, IIT Madras (Retd.) and gave copies to Smt. Rajyalakshmi Ramamurti and Dr. G. Ilavazhagan, Director (Research), Hindustan University, Chennai. Earlier, Dr. V. Bhujanga Rao, President, CMSI delivered the presidential address and gave away certificates to CMSI luminaries while Dr. B. P. C. Rao, Convener, NCCM-2017 gave the welcome address and Dr. P. V. S. Ganesh Kumar, Senior Vice-President, CMSI outlined the condition monitoring society activities and initiatives.

Prof. Amiya Ranjan Mohanty, IIT, Kharagpur and Dr. A. Rama Rao, BARC, Mumbai (Retd.) delivered the keynote talks highlighting the advances and future trends in condition monitoring. Four invited talks and 40 contributory talks were presented. The conference was attended by 130 participants from academia, industry and research. In the valedictory function the participants gave a very good feedback on technical sessions and arrangements.

*B. P. C. Rao  
Convener, NCCM-2017*

## Conference and Meeting Highlights

### 9<sup>th</sup> National Conference on Thermo Physical Properties

November 06-08, 2017



Prof. N. V. Chandra Shekar, Prof. G. Amarendra, Prof. P. R. Vasudeva Rao, VC, HBNI, Prof. Arun Kumar Bhaduri, Director, IGCAR, Prof. N. S. Saxena, President, TPSI and Dr. Awadhesh Mani Tiwari during the release of the souvenir

The 9<sup>th</sup> National Conference on Thermo Physical Properties (NCTP-2017) was held during November 6-8, 2017 at IGCAR, Kalpakkam. The conference was held under the auspices of Thermo Physical Society of India (TPSI), a pioneering society related to research on thermo physical properties of materials, founded in 1999. The series of conferences titled National Conference on Thermo Physical Properties (NCTP) are held once in two years at different locations. The present conference has been supported by IGCAR, BRNS, MRSI and SCSVMV, Kanchipuram.

The conference commenced with the inaugural function. The convener Prof. N. V. Chandra Shekar, Head, CMPD, MSG, IGCAR welcomed the gathering. Prof. N. S. Saxena, President TPSI, deliberated on the history and functioning of TPSI. Prof. G. Amarendra, Chairperson, NCTP stressed the relevance of thermo physical property studies for the myriads of applications in functional materials and elucidation of underlying mechanism in phase transitions. Prof. Arun Kumar Bhaduri Director, IGCAR succinctly pointed out the need to evolve computational algorithms that will model the thermo physical properties of materials during and also immediate post welding scenarios. Prof. P. R. Vasudeva Rao, Vice Chancellor, Homi Bhabha National Institute, Mumbai & Former Director, IGCAR inaugurated the conference and in his lucid inaugural address elaborated the need to place high premium on thermo physical property studies of reactor materials.

Senior scientists and professors from IGCAR, IITs, NITs, IISERs and reputed universities presented invited lectures on their front end research work based on thermo physical property studies. Oral and poster presentations by delegates drawn from across the country showcased their current results. Young scientist achiever, best oral and poster awardees identified by a team of Judges, were honoured by TPSI in the valedictory event. In all, the gathering of about 150 delegates was focused and the discussions in and out of the lecture hall indicated possible future collaborations following NCTP-2017. The concluding ceremony closed with the announcement of the next meet in 2019 as an International event.

*N. V. Chandra Shekar  
Convener, NCTP-2017*



## Conference and Meeting Highlights

### The 2<sup>nd</sup> Research Coordination Meeting of the IAEA Coordinated Research Project (CRP)

November 13-17, 2017



Delegates of IAEA-CRP meeting

The 2<sup>nd</sup> Research coordination meeting of the IAEA Coordinated Research Project (CRP) on "Radioactive Release from sodium-cooled Fast Reactor under Severe Accident Conditions" was organised by IAEA and IGCAR during November 13-17, 2017 at SRI Guest house, Anupuram. The purpose of the CRP is to perform realistic estimation of radio nuclide distribution in primary system coolant and in-containment under severe accident conditions for a reference sodium-cooled fast reactor (SFR). The specific objective is to improve understanding of the key phenomena involved in the release and transport of radioactive material in the reactor vessel and in the containment compartments under severe accident conditions. The studies and modelling exercises are aimed at extending the predictive capabilities of the simulation tools devoted to SFR design and safety analysis. The purpose of this meeting was to review the final benchmark specifications, present and compare calculation models and results and agree on the detailed work programme for the refined simulations. The meeting began with the welcome and introductory address by Shri Vladimir Kriventsev, Scientific Secretary of the CRP, IAEA and opening remarks by Shri P. Puthiyavinayagam, Director, Reactor Design Group and the technical sessions of the meeting were chaired by Shri A. John Arul, Head, RSDD and scientists from IGCAR & SRI. The delegates participated were from IAEA, USA, China, Russia and Japan. This apart few delegates from France, Japan and China participated through video conferencing. There were about 17 presentations on the three work packages defined for the CRP. There has been comparatively more participation in the area of containment phenomena modelling compared to in-vessel source term modelling and main vessel to containment interface modelling. A report of the meet detailing the presentation and discussions of the meeting was also released.

*John Arul*

*Convener, The 2<sup>nd</sup> Research coordination meeting of the IAEA Coordinated Research Project (CRP)*

## Theme Meeting on “Structural Integrity Assessment of Engineering Components

December 5, 2017

The Indian Institute of Metals (IIM), Kalpakkam Chapter organised a half a day Theme Meeting on “Structural Integrity Assessment of Engineering Components” on December 5, 2017 at NDED Auditorium for the benefit of young engineers and scientists. The programme commenced with opening remarks by Dr. G. Amarendra, Distinguished Scientist and Director, MMG & MSG, IGCAR. A series of lectures were delivered by Prof. Shyam Keralavarma, Department of Aerospace Engineering, IIT Madras, Dr. S. Vishnuvardhan, Sr. Scientist, SERC Chennai, Dr. A. Moitra, Head, MMS, MDTD, MMG and Dr. C. K. Mukhopadhyay, Head, NDED, MMG. In this theme meeting, various topics were discussed including modelling of various damage mechanisms, assessment of fracture behaviour of nuclear materials and power plant



Dr. G. Amarendra, Director, MSG & MMG, IGCAR giving the opening remarks

pipework components and the role of non-destructive testing (NDT) techniques for ensuring integrity of engineering components.

C. K. Mukhopadhyay  
Convener, The Indian Institute of Metals (IIM),  
Kalpakkam Chapter

## Visit of Dignitaries



Delegates from CEA with colleagues of the Centre

A delegation from CEA, France led by Dr. Christian Latge, Research Director, NTD visited the Centre on October 3, 2017. The delegation visited the Fast Breeder Test Reactor, KAMINI, Radio Metallurgy Laboratory, facilities in Fast Reactor Technology Group and Reactor Design Group.



Dr. A. Ravisankar, Director, RpG & Project Director, FRFCF, demonstrating the multi pin chopper facility to Dr. M. R. Srinivasan, Member, Atomic Energy Commission and former Chairman, Atomic Energy Commission

Dr. M. R. Srinivasan, Member, Atomic Energy Commission and former Chairman, Atomic Energy Commission, visited Reprocessing Group on November 15, 2017.

## HBNI-IGCAR Corner






Deans from various constituent institutions of HBNI, along with Dr. Arun Kumar Bhaduri, Director, IGCAR & Member Academic Council, HBNI and Dr. P. R. Vasudeva Rao, Vice-Chancellor, HBNI

The 16<sup>th</sup> meeting of the Standing committee of Deans was held on November 06, 2017 at IGCAR, Kalpakkam. Deans from various constituent institutions of HBNI have taken part in the meeting. Dr. Arun Kumar Bhaduri, Member, Academic Council HBNI and Director, IGCAR welcomed the gathering and presented about HBNI activities at IGCAR. The Vice-Chancellor, Dr. P. R. Vasudeva Rao highlighted the various activities of HBNI and discussed about the proposed visit of UGC team to various Constituent Institutions of HBNI. The VC, HBNI mentioned about importance of organizing workshop on scientific writing for doctoral students. Organization of annual Research Scholars' Meet was discussed in detail. The status of former students of HBNI and formation of Alumni Association was deliberated. Enrollment of students and matters relating to on-going academic programs were discussed. Mr. Jehadeesan, Head, CD made a presentation on the software developed at IGCAR for HBNI database. Dr. G. Amarendra, Chairman, Apex committee of HBNI-IGCAR and Dr. S. Sivakumar, IGCAR briefed about the organization of JEST examination at IGCAR.



Visit of UGC-AICTE Team to IGCAR on 30<sup>th</sup> November 2017




Name	Title	Date	Discipline
 Shri Ch. Deepak	Study of Synchro and Development of Synchro-to-Digital Converter for Instrumentation & Control Applications	23.10.2017	Engineering Sciences
 Shri P. Anees	Modeling and Simulations of Structural, Thermal Expansion and Anharmonicity of 2D Materials	27.10.2017	Physical Sciences
 Shri R. Gopi	Experimental Evidence for Blue and Red-shifted Hydrogen Bond: A Matrix Isolation Infrared Spectroscopy and ab Initio Studies	10-11-2017	Chemical Sciences
 Ms. R. Rama	Solvent Extraction and Electrochemical Studies of Lanthanides and Actinides in Room Temperature Ionic Liquid Medium Containing Various Extractants	04-12-2017	Chemical Sciences
 Shri N. Desigan	Chemical Aspects of Dissolution of Fast Reactor Nuclear Fuel	22-12-2017	Chemical Sciences



Oxygen Plasma Treated Vertical Graphene Nanosheets for Supercapacitor Application

Shri Gopinath Sahoo, "International Conference on Nanotechnology: Ideas, Innovations and Initiations - 2017 (ICN:3I-2017)" held at Roorkee during December 6-8, 2017

## DAE Awards



Department of Atomic Energy has instituted annual awards for excellence in Science, Engineering and Technology in order to identify best performers in the area of Research, Technology Development and Engineering in the constituent units (other than Public Sector Undertakings and Aided Institutions). The Young Applied Scientist, Young Engineer, Young Technologist, Homi Bhabha Science and Technology Award and Scientific and Technical Excellence Award fall under this category. Group Achievement awards for recognition of major achievements by groups have also been instituted. Life-time Achievement Award is awarded to one who has made significant impact on the DAE's programmes. They are the icons for young scientists and engineers to emulate. The awards consist of a memento, citation and cash prize.

### The recipients of the Awards from IGCAR for the year 2016 were:

<b>Young Scientist Award</b>	: Dr. Chanchal Ghosh, MMG
<b>Young Applied Scientist/Technologist Award</b>	: Dr. Balija Sreenivasulu, MC&MFCG
<b>Scientific and Technical Excellence Award</b>	: Dr. Arup Dasgupta, MMG Dr. Awadhesh Mani, MSG Shri Sriramachandra Aithal, RDG
<b>Young Engineer Award</b>	: Shri L. Suresh, RDG Shri Ranjit Jovin Cyriac, RDG Shri N. Subramanian, EIG
<b>Meritorious Service Award</b>	: Shri D. M. Raut, RM&PAG Shri G. Munuswamy, CC
<b>Meritorious Technical Support Award</b>	: Shri K. Ellappan, RFG Shri C. S. Rajasekharan Nair, RFG Shri S. Srinivasan, FRTG Shri R. Karunakaran, MC&MFCG

### Group Achievement Awards:

**Development and Qualification of PFBR Steam Generator (PSGIS) and Inspection of Eight Steam Generators (SGs) using PSGIS**  
Shri Joseph Winston, FRTG, Group Leader

Dr. Arun Kumar Bhaduri, Dr. G. Amarendra, Dr. S. Murugan, Dr. B.P.C. Rao, Dr. C.K. Mukhopadhyay, Shri PK. Chaurasia, Shri D. Jegadeesan, Shri S. Sakthivel, Shri P. Visweswaran, Shri Joel Jose, Shri K. Purushothaman, Shri M. Muthuganesh, Shri R. Ravikumar, Shri N. Mahendra Prabhu, Shri Manam Samba Siva Rao, Shri Rajesh Saxena, Shri R. Ramesh, Smt. T. Prabavathy, Dr. S. Thirunavukkarasu, Dr. B. Sasi, Shri V. Arjun, Dr. W. Sharat Chandra Singh, Shri Manoj Kumar Raja, Shri T.K. Haneef and Shri S. Arun Kumar, from **MMG**; Shri S. Athmalingam, Shri R. Sriharan and Shri R. Nandakumar from **RDG**; Shri P. Rajendra Prasad, Shri Vashistha Kumar Pandey, Shri Krishna Chaitanya Gudimella, Shri K. Akilan, Shri V. Rasaram, Shri K. Karthick, Shri B. Vasudevan, Shri E. Manigandan, Shri S. Manickam, Shri S. Sudhakar Naik and Shri B. Maruthan from **BHAVINI**

**Development of Integrated Cold Trap for In Vessel Primary Sodium Purification**

Shri G. Padmakumar, RD, MRPU (then FRTG), Group Leader

Dr. B.K. Nashine, Dr. J.I. Sylvia, Shri S. Chandramouli, Shri V. Ramakrishnan, Shri V. Vinod, Shri G. Vijayakumar, Shri Sarat Kumar Dash, Shri A. Ashok Kumar, Shri Prashant Sharma, Shri S. Ignatius Sundar Raj, Shri R. Rajendra Prasad, Shri Rakesh Kumar Mourya, Shri S.C.S P. Kumar Krovvidi, Shri M.G. Hemanath, Shri S. Krishnakumar, Shri J. Saravanan, Shri M. Anbucheluyan, Shri M. Anandaraj, Shri T.V. Maran, Shri S. Sathishkumar, Shri Vijay Singh Sikarwar, Shri B. Nagaraju,

Shri S. Alexander Xavier, Shri S. Ravishankar, Shri D. Muralidhar, Shri D. Laxman, Shri Chatlal Thakur, Shri N. Venkatesan, Shri Parmanand Kumar, Shri A. Thirunavukkarasu, Shri P.R. Ashokkumar, Shri K. Arumugam, Shri Shaik Rafee, Shri M. Karthikeyan, Shri K. Ganesh, Shri M. Munikumar, Shri S. Ponthilagar, Shri N. Prem Anand, Shri S. Sarvanan, Shri G. Rathnachalam, Shri H. Rafiq Basha, Shri K. Ramesh, Shri V. Krishnamurthy, Shri V. Gunasekaran, Shri M. Kathiravan, Shri K. Mohan Raj, Smt. S. Nagajothi, Shri P. Chenthil Velmurugan, Shri C. Rajappan, Shri N. Sreenivas, Shri L. Eagambaram, Shri N. Mohan, Shri G. Anandan, Shri J. Prem, Shri K. Ravi, Shri A. Kolanjiappan, Shri Vijay Tirkey, Shri K.H. Anub, Shri J. Prabhakaran, Shri Ashish Tiwari, Shri L. Mohanasundaram, Shri L. Muthu, Shri S. Balakrishnan, Shri P. Lakshmayya, Shri P. Pothi, Shri Pitambar Padhan, Shri K.A. Bijoy, Shri A. Selvakumaran, Shri R. Iyyappan, Shri R. Parandaman and Smt. S. Saravana Priya from **FRTG**; Shri Makrand Rajhans from **RMPAG**; Shri S. Athmalingam and Shri V. Krishnamurthy from **RDG**

#### Design, Development and Performance Evaluation of Core Flow Measuring System for FBRs

**Dr. V. Prakash**, **FRTG**, Group Leader

Shri G. Padmakumar, Dr. C. Meikandamurthy, Shri V. Vinod, Shri S. Sureshkumar, Shri Sudheer Patri, Shri Muhammad Sabih, Smt. S. Narmadha, Shri N. Ravichandran, Shri Hadibandhu Singh, Shri C.N. Sridhar, Shri K. Balaji, Shri S. Balakrishnan, Shri Tribhuvan Ram, Shri D. Laxman, Shri M. Kathiravan, Shri V. Gunasekaran, Shri R. Rajendran, Shri N.S. Shivakumar, Shri Nagaraju Bekkenti, Shri K.H. Anub, Shri N. Mariappan, Shri S. Rajkamal Singh, Shri K. Srinivasa Rao, Shri T.V. Maran, Shri K. Mohanraj, Shri A. Anthuvan Clement, Shri Ramesh Kumar Sharma, Smt. S. Saravana Priya, Shri M. Anbuchelian, Shri C. Asokane, Shri S. Chandramouli, Shri P. Centhil Vel Murugan, Shri K. Arumugam, Shri N. Mohan, Shri K. Ramesh, Shri Shaik Rafee, Shri L. Muthu, Shri V. Krishnamoorthy, Shri I.B. Noushad, Shri V.A. Sureshkumar, Shri V.S.P. Babu, Shri K. Thanigairaj, Shri S. Kishore, Shri L.S. Sivakumar, Shri M. Ravishankar, Shri S.P. Pathak, Shri Vishal. D. Paunika, Shri R. Kannan, Shri C.L. Thakur, Shri R.K. Sharma, Shri V. Elumalai, Shri P. Narayana Rao, Shri K.G. Radhakrishnan Unni, Shri K.V.S.S.N. Murthy, Shri V. Saravanan, Shri Sukanta Kumar Roy, Shri S. Suresh, Shri P. Hrishikesh, Shri Tirkey Vijay, Shri M. P. Sunny, Shri K. Sekar, Shri E. G. Prabakaran, Shri K. Sadiqbatcha, Shri N. Premanand, Shri G. Ratnachalam, Shri M. Munikumar, Shri C. Pavaderadjane, Shri A. Saravanan, Shri S. Saravanan, Shri K. Arulselvam, Shri S. Ponthilagar and Shri A. Elumalai from **FRTG**; Smt. R. Vijayashree, Shri B. Madhavan, Shri Sanjeev Kumar and Shri S. Arumugam from **RDG**; Shri K. Sasikumar, Shri K.G. Subramanian, Shri G.N. Chandrasekaran, Shri S. Kanagaraju, Shri B. Balagopal, Shri R. Ramesh, Shri K. Kamaludeen, Shri K. Amos, Shri D. Vinoth, Shri B. Dharmaiah, Shri M. Ganesan, Shri V. Velu, Shri V. Govindaraj, Shri R. Vinoth and Shri V. Rajkumar from **RFG**. Shri G. Kempulraj, Shri B.S. Ramesh Babu. Shri M. Krishnamoorthy, Shri V. Praveen Kumar, Shri S. Parivallal, Shri R. Tamilamuthan, Shri V. Rajendaran, Shri J. Abilash, Shri S. Thiyagu, Shri E. Gothandan, Shri N. Dhanasekaran, Shri V. Kodiarasan, Shri L. Sivakumar, Shri M. Damodharan, Shri A. Gunasekaran, Shri B. Ramalingam, Shri K. Chakarapani, Shri S. Manimaran, Shri S. Ramesh and Shri C. Siva from **ESG**; Shri M. Sakthivel, Shri J. Selva Solomon and Shri A. Nageswaran from **EIG**; Shri M. Karthick from **FRFCF**; Shri Rajeev Ranjan Prasad from **RDG**; Shri B. Anandapadmanaban, Shri N. Raghu, Shri Saju T. Abraham, Shri P. Ramesh, Shri Uma Shankar, Shri B. Govindasamy, Shri D. Hensonraj, Shri K. Murugan, Smt. D. Chitra, Shri Krishna Chaitanya, Shri P. Narayana Rao, Shri D. Kuppusamy, Shri C. Muniyandi and Shri G. Vijaya Raghavan from **HSEG**; Shri M. Tenneyson, Shri M. Vijayaragavan, Smt. H. Rogaiya Banu, Shri J. Ranganathan, Shri M. D. Baktavastchalam and Smt. Padmini Rajan from **MRPU**

#### Development of Online Nuclear Emergency Response (ONERS) Decision Support System for Nuclear Emergency Response and Atmospheric Dispersion of Sodium Aerosols for Evaluation of Chemical Toxicity Towards SFR Safety

**Dr. B. Venkatraman / Dr. R. Baskaran**, **HSEG**, Group Leader

Dr. C. V. Srinivas, Dr. R. Venkatesan, Shri A. Bagavath Singh, Shri P. T. Rakesh, Dr. V. Subramanian, Shri V. Gopalakrishnan, Shri M. Bhupati, Ms. Anju Kumari, Dr. Amit kumar, Ms. Usha Pujala, Ms. Sujatha Pavan Narayanam from **HSEG**; Dr. B. K. Nashine, Shri B. Babu, Shri S. Chandramouli, Dr. J. I. Sylvia, Shri G. Vijayakumar, Shri A. Ashok Kumar, Shri R. Rajendra Prasad, Shri V. Ramakrishnan, Shri S. Krishnakumar, Shri D. Laxman, Shri V. Gunasekaran, Shri M. Kathiravan, Shri C. Rajappan, Shri R. Iyyappan, Shri K. Ramesh, Shri Vijay Tirkey, Shri V. Krishnamurthy, Shri Pitamber Padhan, Shri G. Anandan, Shri L. Muthu, Shri P. Lakshmayya, Dr. R. Ananthanarayanan, Shri M. Manogaran from **FRTG**

## Awards and Honours

Dr. Arun Kumar Bhaduri has been awarded GD Birla Gold Medal (2017) by Indian Institute of Metals on November 14, 2017 at the inaugural function of the 55<sup>th</sup> National Metallurgists' Day Celebrations & 71<sup>st</sup> Annual Technical Meeting of the Institute held at BITS, Pilani, Goa

Dr. Arun Kumar Bhaduri has been conferred with "Doctor of Science" (Honoris Causa) by Jadavpur University, Kolkata based on his "professional contribution to Science and Society, as a whole", at the Convocation program of the University on 24<sup>th</sup> December 2017

Dr. B. Venkatraman delivered "Keynote lecture" on "Towards robust quality assurance through multi modal NDE integrated with modelling, simulation and image/signal analysis" at 15<sup>th</sup> Asia Pacific conference on NDT (15<sup>th</sup> APCNDT), Singapore, held during November 13-17, 2017

Shri A. Manivannan, Shri A.V. Vinod, Shri P. Ravisankar, Shri G. Saravanan, Shri S. Maharajan, Smt. R. Jayshree and Shri Madaka Santhosh of Fermi Quality Circle Team of MFFD, MFRG, MC & MFCG have presented their case study and won the award "Excellent (Silver category)" in the National Convention on Quality Concepts held during December 1-4, 2017 at JSS Science and Technology University, Mysuru

Dr. B. P. C. Rao, MMG received the award for "Best Technical Paper in R&D" from ISNT for the article titled "Multidimensional Basis Function Neural Network for Sizing Flaws from Eddy Current Images" published during 2016 in Journal of Non-destructive Testing & Evaluation, on December 14, 2017

## Best Paper/Poster Award

Compressibility Study of RE<sub>6</sub>UO<sub>12</sub> at Elevated Pressure and Temperature

Shri Balmukund Shukla, Dr. N R Sanjay Kumar, Dr. N. V. Chandra Shekar, Dr. H. Jena and Dr. S. Kalavathi  
9<sup>th</sup> National Conference on Thermophysical properties 2017, held at IGCAR during November 6-8, 2017  
Best Poster Award

High Pressure Spectroscopic Studies of Phase Transition in VO<sub>2</sub>

Ms. Raktima Basu, Shri K. K. Mishra, Dr. T. R. Ravindran and Dr. Sandip Kumar Dhara  
9<sup>th</sup> National Conference on Thermophysical properties 2017, held at IGCAR during November 6-8, 2017  
Best Poster Award

Luminescence Studies in Lithium Fluoride

Dr. U. Madhusoodanan, Shri P. Vinodkumar, Shri S. K. Panda, Shri N. Suriyamurthy and Dr. B. S. Panigrahi  
9<sup>th</sup> National Conference on Thermophysical properties 2017, held at IGCAR during November 6-8, 2017  
Best Paper Award

An Investigation on the Factors Influencing Creep Rupture Life of 316LN SS Weld Joints

Dr. V. D. Vijayanand, Dr. G.V. Prasad Reddy and Dr. K. Laha  
Young Professional International Conference 2017/Weld PCT 2017  
Organized by the International Institute of Welding held at Chennai during December 7-9, 2017  
Best Paper Award

Neutron Radiography Examinations of Advanced Fast Reactor Fuels

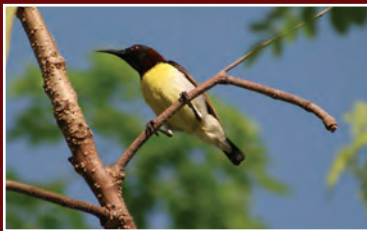
Shri V. Anandaraj, Shri Ran Vijay Kumar, Dr. C. Padma Prabu, Dr. V. Karthik, Shri T. Johny and Dr. R. Divakar  
National Conference on Non-destructive Evaluation–NDE2017 held at Chennai during December 14-16, 2017  
Best Paper Award

# Biodiversity Basket

## Avian Fauna



*Rumpeds'  
sumptuous food on  
a sunny day*



### ***Purple-rumped Sunbird***

Purple-rumped sunbird is seen perching on a plaintain flower. It feeds on nectar from flowers. They are commonly found in South India. They reside and breed in Kalpakkam. Male and female look slightly different.

Editorial Committee Members: Dr. T. S. Lakshmi Narasimhan, Dr. N. V. Chandra Shekar, Dr. C. K. Mukhopadhyay, Dr. Vidya Sundararajan, Shri A. Suriyanarayanan, Dr. C. V. S. Brahmananda Rao, Dr. V. Subramanian, Ms. R. Preetha, Shri J. Kodandaraman, Shri G. Venkat Kishore, Shri S. Kishore, Dr. N. Desigan, Shri M. Rajendra Kumar, Shri V. Rajendran, Ms. S. Rajeswari, Shri K. Ganesan, Shri K. Varathan and Shri G. Pentaiah